Timing synchronization and Frequency offset estimation for Ultra-Wideband (UWB) Multi-Band OFDM systems

YAK CHIN WEE
(M.ENG, NUS)

A thesis submitted
for the degree of Master of Engineering
Department of Electrical & Computer Engineering
National University of Singapore
2005

Acknowledgments

I am extremely thankful to my supervisors Dr. Zhongding Lei and Prof. Thiang Tjeng Tjhung for their timely guidance, patience and encouragement. Deepest gratitude to Dr. Lei especially, thanks to you that I have learnt so much along the way! Appreciation goes out to Mr Suttinan Chattong. Kudos to Ms Wei Ying Lim, for encouraging me all this time.

To my dearest ♡ Mummy, I love you always! Thank you for your selfless love and standing by me all the time. To my faithful companion, Oscar for all the late nights you stayed up by my side. ✌

Summary

This thesis deals with symbol timing synchronization and carrier frequency offset estimation under multi-band orthogonal frequency division multiplexing (MB-OFDM) ultra-wideband (UWB) systems in frequency selective fading channels.

First, a timing synchronization algorithm: First significant multipath detection via Threshold comparison of Adjacent samples (FTA) is proposed to exploit the dedicated periodic training sequences by comparing the difference between adjacent samples of a proposed metric against a pre-defined threshold. This metric is obtained from accumulating the energies of various multipath components (MPCs) at the receiver while noise is simultaneously averaged to nil as more MPCs are summed. The threshold is chosen based upon initial measurements of the environment's signal-to-noise ratio (SNR). The simulated UWB channel models (CMs) are: UWB CM Line-of-sight (LOS) 0-4m (CM1) and UWB CM Non-line-of-sight (NLOS) 0-4m (CM2) as specified by the IEEE 802.15.3a task group [11]. Three correlation algorithms extended from conventional orthogonal frequency division multiplexing (OFDM) systems are presented for comparison. The proposed FTA algorithm is at least 75% more accurate than the next best algorithm in terms of mean squared error and at least 53% more likely to achieve timing synchronization in terms of synchronization probability under a typical operating signal-to-noise ratio (SNR) of 17 dB.

The maximum likelihood (ML) frequency offset (FO) estimator variance and the Cramer Räo Bound (CRB) are derived for the MB-OFDM UWB system. They serve as lower bounds against which the proposed FTA FO estimator variance is benched. The FTA FO estimation algorithm is extended from the proposed metric whereby the phase differences between each subcarrier of two adjacent identical training symbols are extracted and averaged to yield the FTA FO estimator. The FTA FO estimator variance has a SNR loss of less than 0.5 dB compared against the maximum likelihood (ML) estimator variance for both UWB CMs. Further, the ML estimator variance converges to the CRB towards the high SNR end.

Contents

List of Figures

List of Tables

Acronyms

AWGN additive white Gaussian noise

BER bit error rate

CDMA code division multiple access

CE channel estimation sequence

CM channel model

CM1 UWB CM Line-of-sight (LOS) 0-4m

CM2 UWB CM Non-line-of-sight (NLOS) 0-4m

CP cyclic prefix, 32 null samples before *pattern*

CR total number of channel realizations

CRB Cramer Räo Bound

FCC Federal Communications Commission

FFT Fast Fourier Transform

FO frequency offset

FS frame synchronization sequence

FTA First significant multipath detection via Threshold comparison between Adjacent samples

G guard, 5 null samples after *pattern*

ICI intercarrier interferences

IFFT Inverse Fast Fourier Transform

ISI intersymbol interference

MB-OFDM multi-band orthogonal frequency division multiplexing

ML maximum likelihood

MPC multipath component

MSE mean squared error

OFDM orthogonal frequency division multiplexing

PS packet synchronization sequence

RF radio frequency

SNR signal-to-noise ratio

TFC time-frequency code

TO timing offset

TSF time-domain spreading factor

UWB ultra-wideband

Nomenclature

Δ_f	Subcarrier frequency spacing
ϵ	Normalized frequency offset w.r.t. Δ_f
$\hat{d}$	Estimated d_0 time sample
λ	Threshold used in FTA timing synchronization algorithm
$\otimes$	Convolution operation
σ_n^2	Variance of a complex additive white Gaussian noise (AWGN) random variable
σ_s^2	Average transmitted signal power per preamble subcarrier averaged across one *period*
σ_s^2	Average transmitted signal power per preamble subcarrier averaged across one *period*
θ	Timing offset in units of OFDM samples
$\vec{h}$	Channel impulse response
$\vec{p}$	Desired user's preamble *pattern*
$\vec{r}$	Received signal waveform after passing through channel
$\vec{s}$	Transmitted signal preamble
b_k	Polarity of the k^{th} *period*
d	Time domain integer sample index
d_0	Timing instant corresponding to the 1st sample of FFT window in the 1st FS
J	Fisher information
L	Number of PS and FS available for timing synchronization and FO estimation before CE
l	Channel length
len	*Period* duration of in units of OFDM samples
M	Number of data, pilot and guard subcarriers per OFDM symbol
N	Size of FFT or *pattern* duration in units of OFDM samples
n	Complex AWGN random variable
pattern	A sequence of 128 pre-defined preamble values as given in Appendix 5
period	A collective of CP, *pattern* and G as one unit
T_{CP}	Cyclic prefix (CP) duration in seconds
T_{FFT}	Inverse Fast Fourier Transform (IFFT)/Fast Fourier Transform (FFT) duration in seconds
T_G	Guard interval (G) duration in seconds
T_{SYM}	*len* duration in seconds

Chapter 1

INTRODUCTION

Ultra-wideband (UWB) is a technology that promises to deliver high data rates of up to 480 Mbps for short distances in practical wireless environments while consuming very little power and silicon estate. The Federal Communications Commission (FCC) has allocated 7500 MHz of spectrum from 3.1 GHz to 10.6GHz for use by UWB devices. The FCC defines UWB as any wireless transmission scheme that occupies a bandwidth of more than 500MHz in the 3.1 to 10.6 GHz band.

1.1 Descriptions of UWB systems

Given the huge bandwidth, there are several approaches to utilize this for system design. The three main champions are "carrierless" pulse-based UWB, code division multiple access (CDMA) UWB and multi-band orthogonal frequency division multiplexing (MB-OFDM).

The conventional pulse-based approach involves developing, transmitting and receiving an extremely short duration burst of radio frequency (RF) energy - typically of a few nanoseconds to picoseconds in duration. The resultant waveforms have extremely wide bandwidths such that it is very difficult to determine the actual carrier frequency - thus termed "carrierless". The impulse is typically generated by impulse or step-excited antennas and filters. The main advantages of this system are low cost and complexity as minimal RF electronics allow for a near "all-digital" design. Some disadvantages include difficulties in collecting significant multi-path energy using a single RF signal; strict switching time requirements (less than 100 ps) at both transmitter and receiver; the receiver signal processing is very sensitive to group delay variation introduced by analog front-end components; and spectral resources are potentially wasted in order to avoid narrowband interferences.

An alternative approach is to use spread spectrum or CDMA techniques. Each data symbol is represented by a code unique for each user and the system bandwidth is determined by the chip

(bit within the code sequence) length which is much shorter than the data symbol length. As different users use different sequences, it is easy to distinguish between users. The main advantage of CDMA based UWB are that spread spectrum techniques are well understood and have been proven in other commercial technologies e.g. wideband CDMA and CDMA2000. However, the downside is that building RF analog circuits and high speed analog-to-digital converters (ADCs) to process this extremely wide bandwidth signal is difficult. Also, digital complexity of the RAKE receiver needs to be large in order to capture sufficient multi-path energy to meet the range requirements of 10 meters for a 110 Mbps system.

Another method is to divide the 7500MHz spectrum into fourteen 528 MHz bands whereby information is transmitted using OFDM modulation on each band:- multi-band orthogonal frequency division multiplexing (MB-OFDM). The fourteen bands are organized into 5 band groups: four groups of three bands each and one group of two bands. Band group 1 is used for mandatory mode 1 devices and the remaining band groups are reserved for future use. OFDM carriers are efficiently generated using an 128-point Inverse Fast Fourier Transform (IFFT) or Fast Fourier Transform (FFT) operation. Information is coded across all bands in use to exploit frequency diversity and provide robustness against multi-path and interference. The multiple bands allow for a high degree of flexibility whereby bands and tones can be dynamically turned on or off for enhanced coexistence with other devices as well as comply with constantly changing world-wide regulations. OFDM is also well understood and has been proven in other commercial technologies e.g. IEEE 802.11a/b/g. Other advantages include relaxed switching times, insensitivity to group delay variations, and the ability to deal with narrowband interference at the receiver without having to sacrifice data rate. The drawback of this system is that the transmitter is slightly more complex because it requires an IFFT/FFT and hence the most costly solution amongst the three approaches.

1.2 Research motivation

In view of the various advantages of multi-band orthogonal frequency division multiplexing (MB-OFDM) over the pulse-based and CDMA approaches for the UWB system, the UWB system considered in this thesis is multi-band orthogonal frequency division multiplexing (MB-OFDM). Timing synchronization and frequency offset estimation at the receiver are very important steps for MB-OFDM. Timing errors can cause intersymbol interference (ISI) that destroys the orthogonality of the OFDM subcarriers and degrades the system performance [1]. Besides ISI, channel estimation will also be affected by the timing misalignment and drag down overall system performance [2].

Frequency offset (FO) arises from a number of factors: random Doppler frequency shifts, carrier frequency mismatch between transmitter and receiver oscillators and sampling frequency error between the ADCs. The FO causes severe reduction in signal amplitude and introduces intercarrier interferences (ICI) from the other subcarriers. As subcarriers are spaced out over the channel bandwidth, the FO must be minimized to a small fraction of the inter-subcarrier spacing in order to avoid severe bit error rate (BER) degradation from these detrimental effects [3]. This thesis focuses on FO from carrier frequency mismatches and Doppler shifts only.

1.3 Literature reviews

There have been many papers on timing synchronization, carrier frequency offset (FO) estimation algorithms as well as joint timing and FO estimation algorithms for various channels and systems. Numerous literature on maximum likelihood (ML) FO estimation and CRB were available too. All the works mentioned below were for conventional OFDM systems instead of the UWB system.

Classen [2] proposed a metric which jointly estimate the timing position and frequency offset by searching for periodic signal structures of OFDM systems over frequency selective multipath channels.

For maximum likelihood (ML) frequency offset (FO) estimation, Moose [3] presented a ML FO estimator calculated in the frequency domain using two repeated symbols. Each symbol is preceded by a portion of the data symbol (cyclic prefix). Simulations are carried out for uniformly distributed selective Rayleigh fading channels.

Schmidl and Cox [4] used a two-symbol training sequence to achieve timing and frequency acquisition. The first symbol has two identical time domain halves on which a correlation based timing metric is applied for estimating the start of FFT window and fractional frequency offsets. Correlation with a second symbol then is performed to resolve any frequency offset ambiguities. A parallel can be drawn from [4] since UWB time domain *periods* are repetitive as well. However, this metric still depended on multipath component (MPC) signal strengths and their channels' had exponential power delay profiles. Stronger delayed MPCs will yield false timing lock-on as well. The CRB for their system of two training symbols under a frequency selective channel with an exponential power delay profile are also presented.

Morelli and Mengali proposed a number of frequency offset (FO) estimation algorithms for OFDM systems [5], [6] and [7]. An extension of [4] is presented in [5] whereby one training symbol consisting of multiple identical parts is used, assuming timing information is available. Since each identical part

in the MB-OFDM UWB preamble has 165 samples, it will be unsuitable to apply the approach in [5] directly on MB-OFDM UWB system as the complexity increases together with the need for a large and hence expensive FFT block for implementation. Algorithms to resolve frequency ambiguities are also published by Morelli and Mengali in a later paper [6]. The maximum likelihood (ML) criterion is also used in [7] for both arbitrary and periodic training sequences.

Minn [8] proposed a timing synchronization algorithm which used one specifically designed training symbol which has a steep roll-off timing metric trajectory for time-varying multipath Rayleigh fading channels. For FO estimation, Minn used a modified approach from [5] as well.

Huang [9] proposed a ML FO estimator which exploited the designation of odd subcarriers as null subcarriers in one OFDM training symbol. Simulations were done for exponentially decaying Rayleigh fading channels.

Van de Beek [10] presented a joint ML symbol-time and FO estimator whereby redundant information within the cyclic prefix are utilized. UWB preambles are designed with null cyclic prefixes instead and hence [10] cannot be applied.

1.4 Contributions of the thesis

In this thesis, the receiver is assumed to have already detected presence of the signal and can thus proceed on with symbol timing synchronization i.e. finding an estimate of where the FFT window starts, using user-unique preambles or repeated training sequences [11]. The proposed algorithm FTA focuses on detecting the first significant multipath component by comparing the difference between two adjacent energy samples of a proposed metric against a pre-defined threshold. Each energy sample is obtained from summing received MPCs' energies. When the threshold is crossed, FTA locks-on to the first significant MPC and deduces the correct symbol timing instant. Three correlation algorithms extended from conventional OFDM systems are also presented for comparison. The proposed FTA algorithm is at least 75% more accurate than the next best algorithm in terms of MSE and at least 53% more likely to achieve timing synchronization in terms of synchronization probability under a typical operating signal-to-noise ratio (SNR) of 17 dB.

Using this timing information, the maximum likelihood (ML) frequency offset (FO) estimator and its theoretical Cramer R*äo* Bound (CRB) for the MB-OFDM UWB system are derived for frequency selective fading channels from the log likelihood function and Fisher information. Simulations are carried out for the two UWB channel models as proposed in [12] with the repeated training sequences.

A simplified FO estimator is extended from the proposed metric by averaging the phase differences between each corresponding subcarrier of the two identical adjacent training symbols. The performance of the proposed FTA FO estimator variance against the ML estimator variance shows less than 0.5 dB SNR loss.

1.5 Thesis Organization

The remainder of this thesis is organized as follows. Chapter 2 describes the multi-band orthogonal frequency division multiplexing (MB-OFDM) ultra-wideband (UWB) system considered, the preamble structure and the UWB channel models (CMs) adopted. The effects of symbol timing error and frequency offset error are also presented.

Chapter 3 focuses on symbol timing synchronization. Three timing synchronization correlation-based algorithms extended directly from conventional OFDM systems are presented followed by the proposed algorithm: First significant multipath detection via Threshold comparison between Adjacent samples (FTA) which is discussed in detail. Its performance is compared against the three conventional OFDM algorithms via simulations and the results discussed.

Chapter 4 first derives the maximum likelihood (ML) frequency offset (FO) estimator and the theoretical Cramer R*äo* Bound (CRB) for multi-band orthogonal frequency division multiplexing (MB-OFDM) ultra-wideband (UWB) system. These serve as a basis for comparison with the proposed FTA FO estimator which is derived later. Its performance is compared against the ML FO estimator variance and its CRB benchmarks.

Finally, Chapter 5 concludes the thesis.

Chapter 2

SYSTEM DESCRIPTION

2.1 Multi-band orthogonal frequency division multiplexing (MB-OFDM) specifications

The MB-OFDM UWB system employs OFDM using a total of M modulated data, pilot and guard subcarriers out of a total of N subcarriers for all bands. Within band group 1 or mode 1, a time-frequency code (TFC) is used to spread data over three frequency bands with each band occupying $\Delta_f N$ bandwidth where Δ_f is the frequency spacing between two adjacent subcarrriers. The MB-OFDM Task Group 3a [11] specified that M, N and Δ_f be of values 122, 128 and 4.125 MHz respectively. Also, a time-domain spreading factor (TSF) of two is used, i.e. transmitting the same information over two OFDM symbols which may or may not belong to the same frequency band. Time-frequency spreading facilitates multiple user access as each logical channel or piconet is defined by its unique TFC. The information is spread across three frequency bands to exploit frequency diversity and provide robustness against multipath and interference. The first band is commonly used by five out of seven TFCs to facilitate the reception of beacon frames by user devices and hence aid their synchronization. The time frequency codes and their associated preamble sequences are defined in Table 2.1 below.

For example, if the device uses a TFC of [1 2 3 1 2 3], the information in the first OFDM symbol is repeated on sub-bands 1 and 2, the information in the second OFDM symbol is repeated on sub-bands 3 and 1, and that of the third OFDM symbol repeated in sub-bands 2 and 3.

Table 2.1: Time frequency code TFC and associated preamble *patterns*

TFC Number	Preamble Patterns	Length 6 TFC					
1	1	1	2	3	1	2	3
2	2	1	3	2	1	3	2
3	3	1	1	2	2	3	3
4	4	1	1	3	3	2	2
5	5	1	1	1	1	1	1
6	5	2	2	2	2	2	2
7	5	3	3	3	3	3	3

2.2 Preamble structure

Dedicated training sequences or preambles are used for timing synchronization, carrier frequency offset recovery and channel estimation. They are designed to have low cross correlation and easy implementation. The preamble signals are defined as real signals at the baseband in order to correspond to the real signals at baseband for the lowest data rate modes. The standard preamble consists of three portions: 21 packet synchronization sequence (PS), 3 frame synchronization sequence (FS) and 6 channel estimation sequence (CE). Figure 2.1 to Figure 2.3 show the structure of the preambles for the different TFCs. By pre-appending 32 null samples (CP) and appending 5 null guard samples (G) to a *pattern* $\vec{p}$ of 128 samples , the combined 165 samples are henceforth defined as a *period* of *len* samples. The FFT window of size N corresponds to the 128 samples. The various preamble *patterns* can be found in the Appendix Tables 5.1 to 5.5. Preambles for the other TFCs have merely different *period* polarity *patterns* and PS, FS arrangements.

In addition to the standard preamble, a streaming mode preamble is also defined. For data rates of 200 Mbps and lower, all packets in the burst use the standard preamble. For data rates higher than 200 Mbps, the first packet uses the standard preamble while the remaining packets use the streaming mode preamble. The streaming mode preambles are similar to the standard mode preambles, also with three portions: 9 PS, 3 FS and 6 CE.

The timing parameters associated with MB-OFDM are summarized as shown in Table 2.2 below.

2.3 UWB channel description

UWB channel measurement and modeling is still a fairly recent field. A reliable channel model which captures the important characteristics of the channel is vital. The IEEE 802.15.3a task group has adopted a modified Saleh-Valenzuela (S-V) channel model [13] with a lognormal amplitude dis-

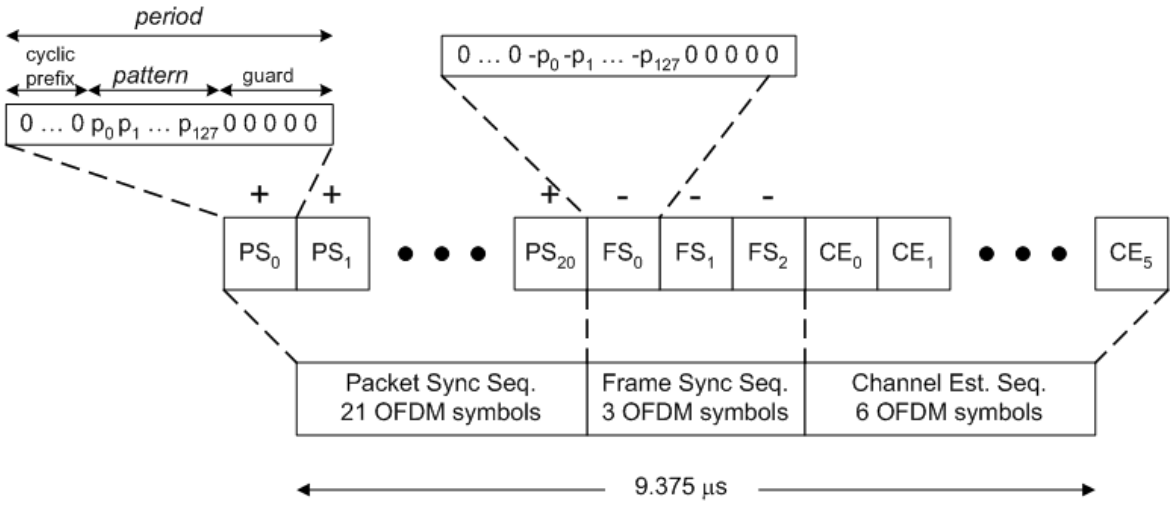

Figure 2.1: Standard preamble for TFCs 1 and 2

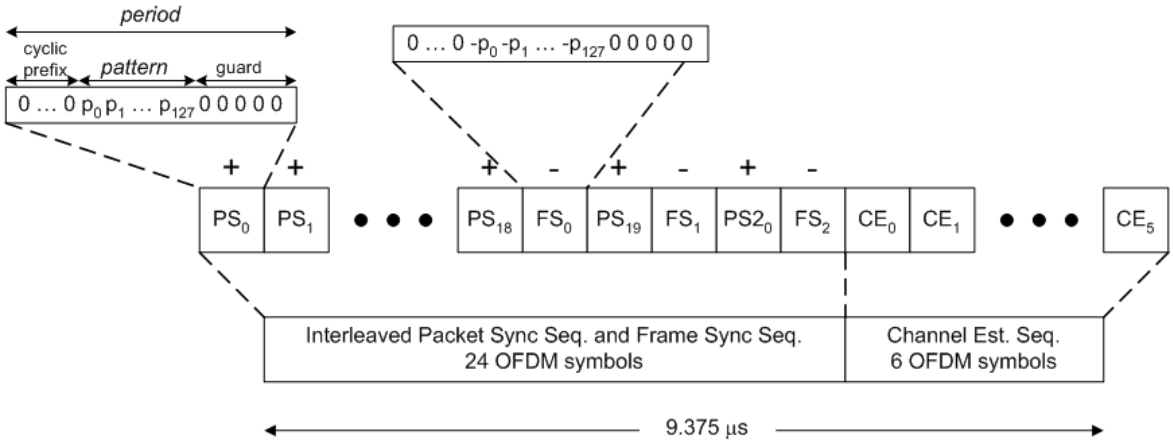

Figure 2.2: Standard preamble for TFCs 3 and 4

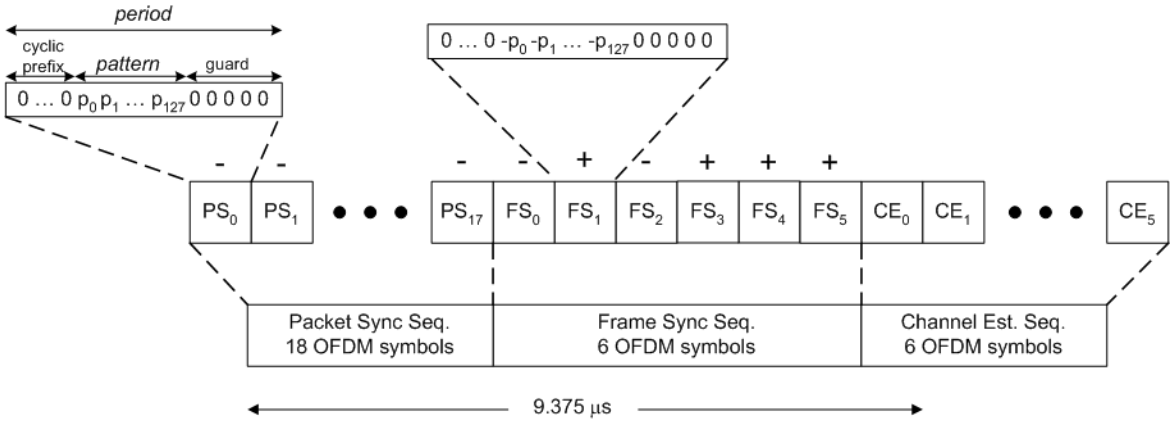

Figure 2.3: Standard preamble for TFCs 5, 6 and 7

Table 2.2: Timing-related parameters

Symbol:	**Parameter description**	**Value**
N	: IFFT/FFT size	128 subcarriers
len	: Symbol size	165 subcarriers
Δ_f	: Subcarrier frequency spacing	4.125 MHz (= 528 MHz/128)
T_{FFT}	: IFFT/FFT duration	242.42 ns ($= 1/\Delta_f$)
T_{CP}	: Cyclic prefix duration	60.61 ns (= 32/528 MHz)
T_G	: Guard interval duration	9.47 ns (= 5/528 MHz)
T_{SYM}	: Symbol duration	312.5 ns ($= T_{CP} + T_{FFT} + T_G$)

tribution [12], [14] that seemed to best fit the channel measurements. The UWB CM is cluster based. A schematic representation of the S-V model is shown in Figure 2.4 to illustrate clusters and rays.

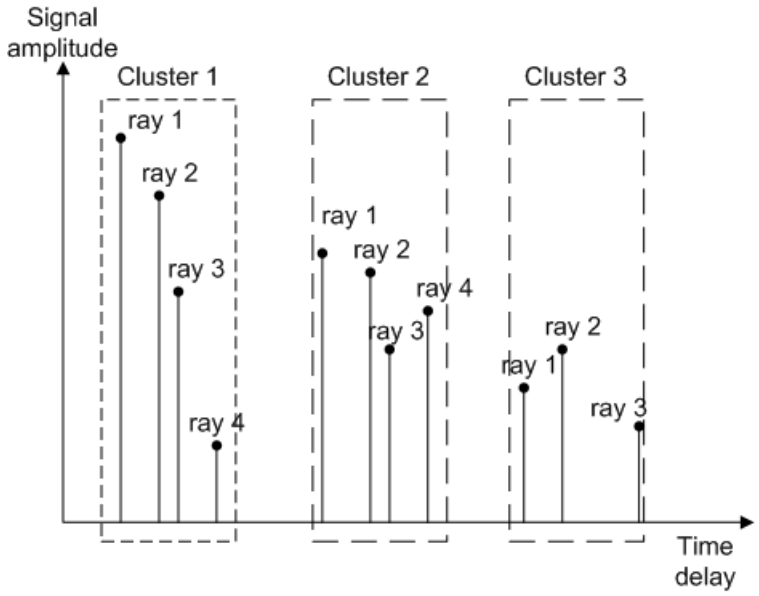

Figure 2.4: Schematic representation of S-V model

UWB channel measurements indicate a lognormal shadowing with the independent fading of rays or multipath components (MPCs) following a lognormal distribution. MPCs' arrival times are modeled using Poisson arrival process and they are grouped into cluster arrival and ray arrival within a cluster.

Let the UWB channel impulse response be denoted by

$$\vec{h} = \{h_0, h_1, \ldots, h_{l-1}\} \tag{2.1}$$

where l is the channel impulse response length in terms of OFDM samples.

2.4 Effects of timing offsets

There are two types of symbol timing offsets: one towards the CP and the other away from the CP. Let the timing index be denoted as d. The timing offset is defined as

$$\theta = \hat{d} - d_0 \tag{2.2}$$

where $\hat{d}$ is the estimated timing instant and d_0 is the correct timing instant corresponding to the first sample of FFT window in the first negative polarity *period* FS.

For a general OFDM system with cyclic prefix (CP), in the case corresponding to timing offset towards CP for d_0 within CP region i.e. $-(CP - l) \leq \theta < 0$ as shown in Figure 2.5, there is no ISI. For timing offset away from CP as shown in Figure 2.6, $\theta > 0$ and there is ISI with the CP of $(i+1)^{th}$

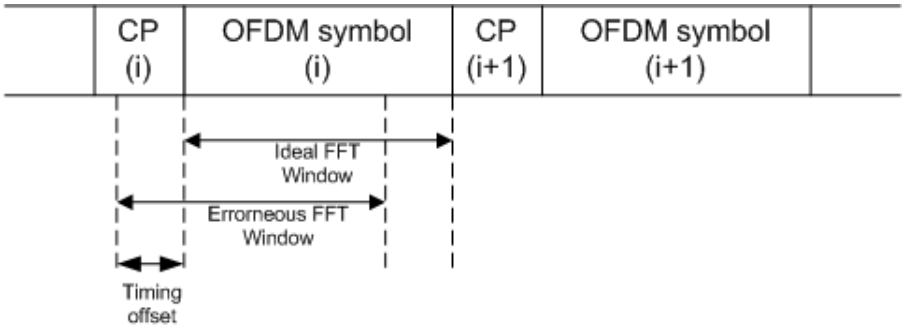

Figure 2.5: Symbol timing error towards cyclic prefix (CP) for the i^{th} OFDM symbol

symbol. For perfect FFT window alignment or no timing offset, $\theta = 0$.

Using the circular shift property of FFT, for a timing offset of $-(CP - l) \leq \theta < 0$, the k^{th} subcarrier experiences a phase shift of $2\pi k\theta/N$ in the frequency domain where N denotes the FFT size. However, when $\theta > 0$ the k^{th} subcarrier experiences both ISI and a phase shift of $2\pi k\theta/N$ in

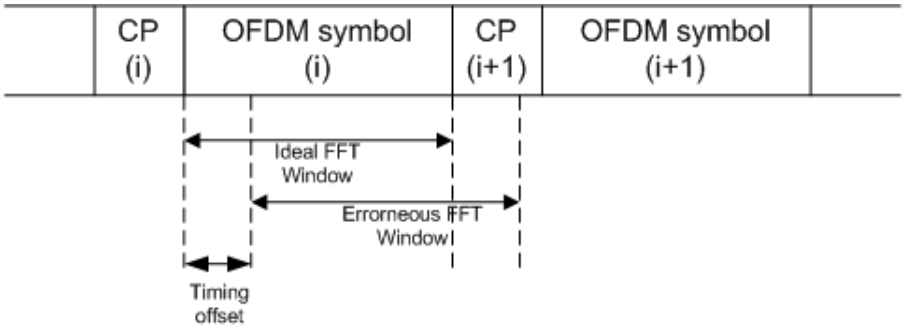

Figure 2.6: Symbol timing error away from CP for the i^{th} OFDM symbol

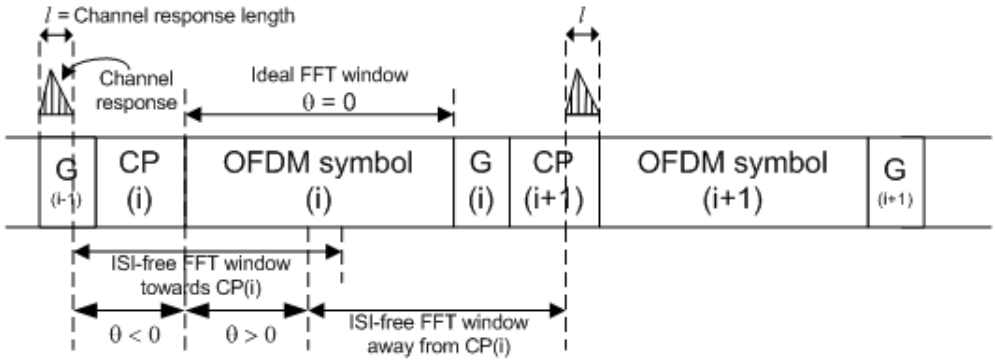

Figure 2.7: Timing errors for MB-OFDM UWB system for the i^{th} OFDM symbol

the frequency domain. This combination of interference significantly worsens BER performance [1].

For MB-OFDM UWB system, the null subcarriers of CP and guard intervals help to increase the ISI-free regions such that timing synchronization requirements can be less stringent. Figure 2.7 illustrates the possible ISI-free windows for both cases of timing offset. The ISI-free region is given by $|\theta| \leq CP + G - l$.

2.5 Effects of frequency offsets

Similarly, frequency offset (FO) manifests itself in the form of an additional phase shift in the time domain. In conventional narrowband OFDM systems, FO is severely detrimental to system performance since the subcarriers are very closely spaced within a small bandwidth resulting in a very small tolerable FO. FO not only reduces the signal strength at the receiver but also introduces intercarrier interferences (ICI) since subcarriers are no longer orthogonal. A detailed derivation of the signal amplitude reduction and intercarrier interferences resulting from FO is presented in [3].

2.6 OFDM system model

For a single frequency band, the transmitted preamble in time domain is given by:

$$\vec{s} = \{\underbrace{PS, \ldots, PS, FS}_{L}, CE, CE\} = \{\ldots, s_d, s_{d+1}, \ldots\} \tag{2.3}$$

where L is a system parameter which denotes the number of PS and FS *periods* before CE and d is the integer time index. After passing through a bandpass channel, the ideal received signal waveform,

$\vec{r} = \{\ldots, r_d, r_{d+1}, \ldots\}$ can be expressed as

$$\begin{aligned} r_d &= s_d \otimes h_d + n_d \\ &= \sum_{i=0}^{l-1} s_{d-i} h_i + n_d \end{aligned} \tag{2.4}$$

where $\vec{h} = \{h_0, h_1, \ldots, h_{l-1}\}$ denotes the channel impulse response, l is the channel length, $\otimes$ denotes the convolution operation and n_d denotes a complex additive white Gaussian noise (AWGN) random variable with zero mean and variance σ_n^2.

In practice, the presence of timing and frequency offsets result in the actual received signal

$$r_d = \sum_{i=0}^{l-1} s_{d-i-\theta} h_i e^{\frac{j2\pi\epsilon d}{N}} + n_d \tag{2.5}$$

where ϵ denotes the normalized frequency offset with respect to inter-subcarrier frequency spacing (Δ_f), i.e. $\epsilon = f_0/\Delta_f$ where f_0 is the actual frequency offset in Hertz.

Chapter 3

SYMBOL TIMING SYNCHRONIZATION

Initially, other than the desired user's TFC and preamble sequence, the time-frequency interleaved channel timing information is not available to the receiver. Hence, focusing on mode 1, the receiver has to stay at one band to receive at least 1/3 of the symbols; otherwise, information chasing and hopping from band to band could happen, and nothing will be received. Besides estimating the correct symbol timing, the start of CE needs to be gauged as well. The negative polarity *periods* of FS serve as clear demarcation points. In this thesis, we focus on synchronizing with the first negative polarity *period* FS where d_0 denote the first sample of its FFT window.

3.1 Overview of symbol timing synchronization algorithms

Three conventional OFDM-extended correlation algorithms are presented as a basis for comparison. The first and second synchronization methods, N-Peak and S-Peak, operate on the resultant waveform after a simple time-domain correlation of the received signal with the desired user's preamble sequence to distinguish between multiple users. N-Peak involves detecting a negative peak in the resultant waveform while S-Peak exploits the known preamble symbol pattern and sums up samples at regular intervals.

The third and fourth synchronization methods, E-Peak and the proposed algorithm: First significant multipath detection via Threshold comparison between Adjacent samples (FTA), kicks in after energy accumulation so as to collect as much multipaths' energies as possible. Noise will be averaged out as more samples are accumulated. E-Peak detects the maximum accumulated energy and translates that timing for the correct symbol timing. The proposed FTA algorithm estimates the correct

timing instant whenever the difference between two consecutive samples after energy accumulation exceeds a pre-determined threshold.

The working signal model for timing synchronization is

$$r_d = \sum_{i=0}^{l-1} s_{d-i-\theta} h_i + n_d \tag{3.1}$$

again where d is the time integer index, $\vec{r} = \{\ldots, r_d, r_{d+1}, \ldots\}$ is the received signal waveform, $\vec{s} = \{\ldots, s_d, s_{d+1}, \ldots\}$, $\vec{h} = \{h_0, h_1, \ldots, h_{l-1}\}$ denotes the channel impulse response, l is the channel length and n_d denotes a complex AWGN random variable with zero mean and variance σ_n^2.

Further details regarding the decision rules and inadequacies of each of the three conventional algorithms are presented. Their performances are evaluated against the proposed FTA algorithm under UWB channel conditions by simulations.

3.1.1 Negative Peak (N-Peak) algorithm

After time-domain correlation of received signal with user's preamble *pattern*, the desired user's signal is retrieved with signal peaks where the *patterns* are aligned. This serves to filter away other users' interference as well as noise. The resultant waveform is expressed as:

$$C_d = \sum_{\substack{k=d \\ m=0}}^{\substack{k=d+N-1 \\ m=N-1}} r_k p_m^* \tag{3.2}$$

where * denotes a complex conjugate operation, $\vec{r}$ is the received signal, $\vec{p} = \{p_0, p_1, \ldots, p_{N-1}\}$ is the desired user's preamble *pattern* and d is the time domain sample (integer) index of the received signal. The estimated synchronization point, $\hat{d}$, is the minimum-valued sample point, i.e.

$$\hat{d} = \min_{\forall d \in \mathbb{Z}} (C_d) \tag{3.3}$$

Figure 3.1 and Figure 3.2 show the waveforms obtained from one particular UWB channel realization under noiseless conditions for CM1 and CM2 respectively. In the Figure 3.1, the FS window happened to still carry a negative polarity after passing through the channel; there is an equally likely chance that the FS window may be converted into positive polarity by the channel as shown in Figure 3.2. Hence, the decision rule to estimate d_0 by Equation (3.3) is only half as accurate as it is difficult to predict the polarity. Timing synchronization performance is expected to be poor.

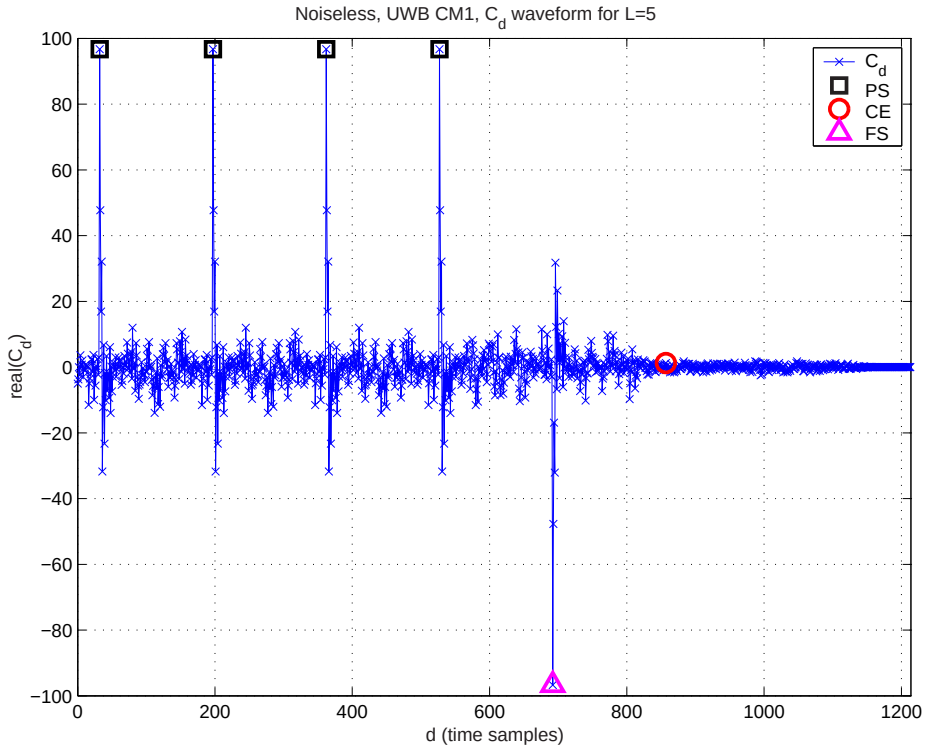

Figure 3.1: C_d for one channel realization under noiseless conditions for UWB CM1

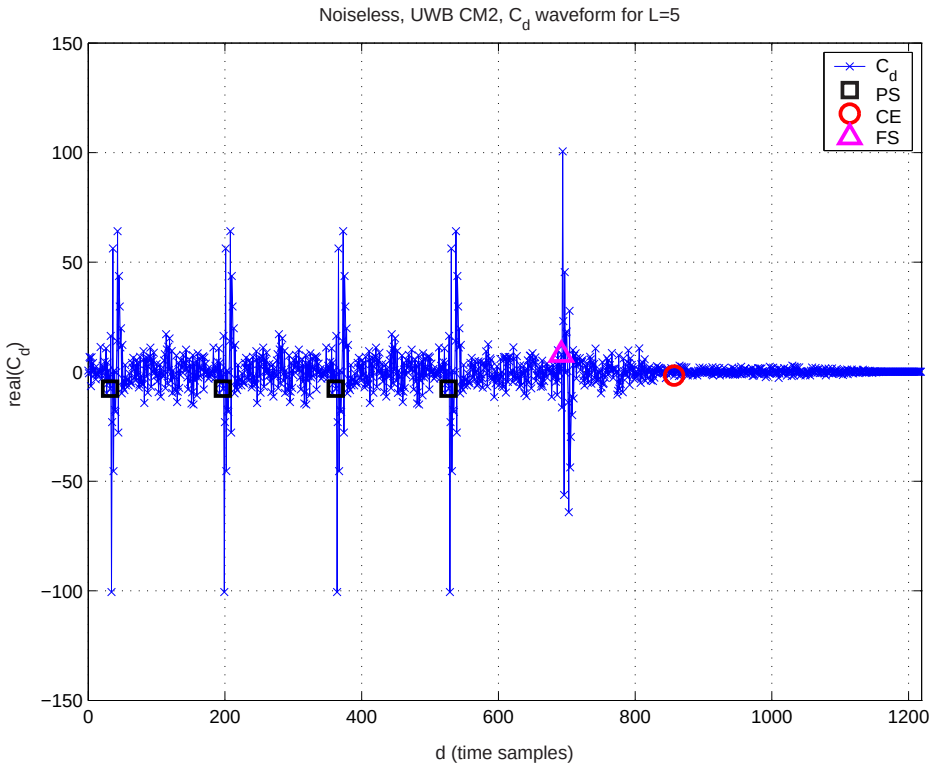

Figure 3.2: C_d for one channel realization under noiseless conditions for UWB CM2

3.1.2 Summation of Peaks (S-Peak) algorithm

This method involves the summation of sample values separated by intervals of *len* samples. Since the polarities of the preamble *periods* are known prior to the receiver, this knowledge can be used to constructively sum all the peaks arising from earlier correlation.

$$S_d = \sum_{k=1}^{L} C_{d+(k-1)len} b_k \tag{3.4}$$

where L is the number of *periods* considered as mentioned in Section 2.6 and $\{b_k : k = 1, ..., L\}$ denote the polarities of the *periods*. The same problem predicting polarities occur here again and it is "resolved" by using the decision rule in Equation (3.5) below instead. Figure 3.3 and Figure 3.4 show the waveforms of Equation (3.4) after taking absolute value of S_d, obtained from one particular UWB channel realization under noiseless conditions for CM1 and CM2 respectively.

$$\hat{d} = \max_{\forall d \in \mathbb{Z}} (|S_d|) \tag{3.5}$$

However, this method cannot estimate the start of the channel estimation sequence, only the correct symbol timing instant. Hence the timing synchronization is not fully achieved.

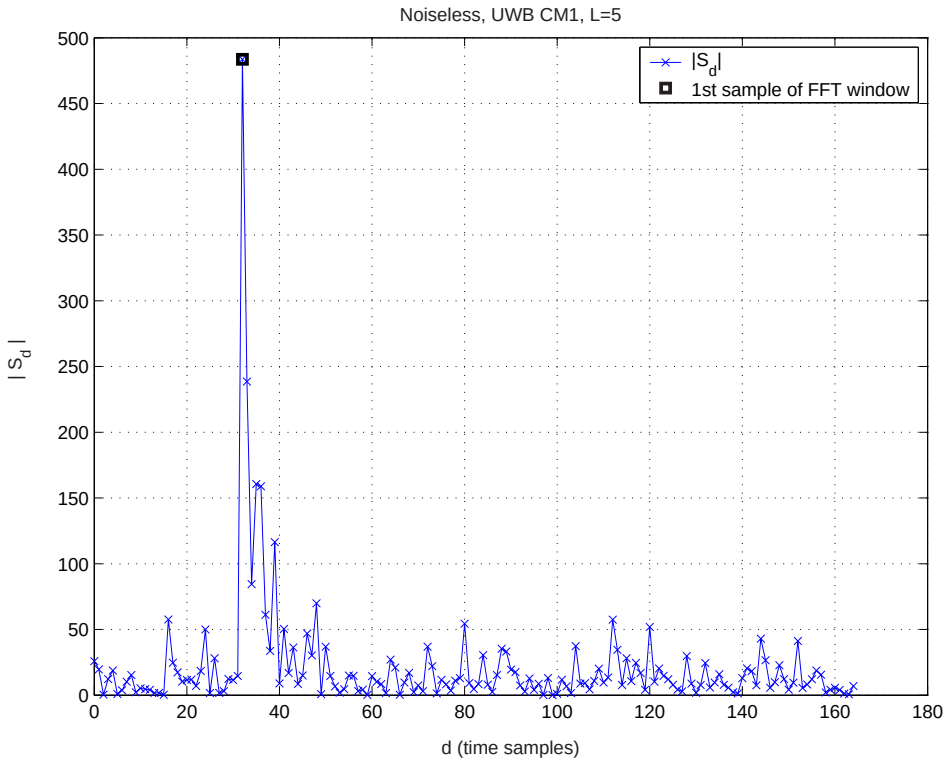

Figure 3.3: $|S_d|$ for one channel realization under noiseless conditions for UWB CM1

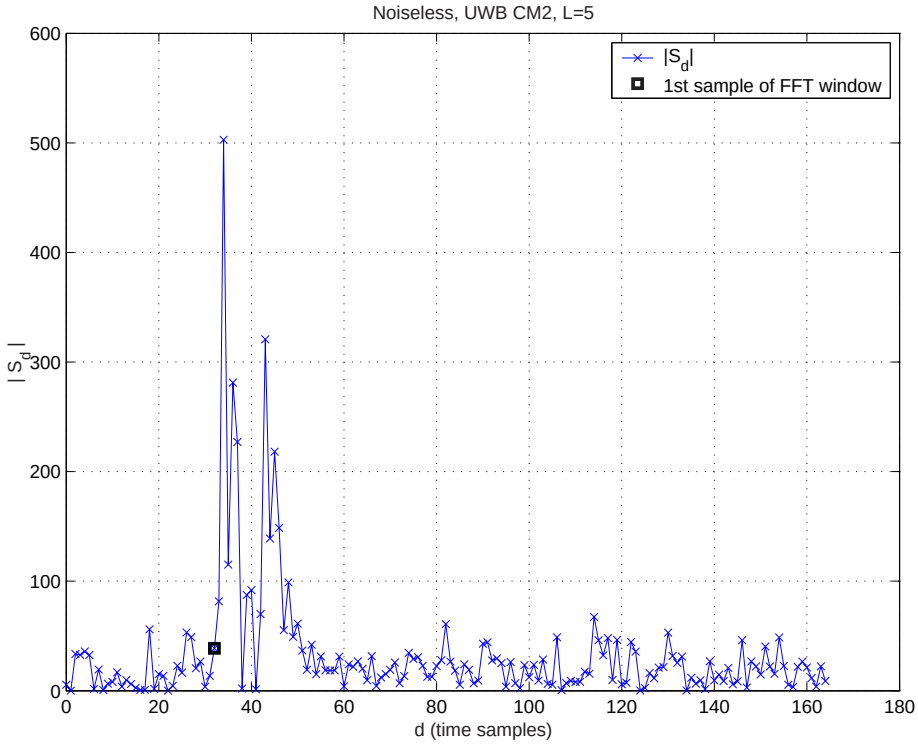

Figure 3.4: $|S_d|$ for one channel realization under noiseless conditions for UWB CM2

3.1.3 Energy Peak (E-Peak) algorithm

Using N-Peak, the decision rule is less than accurate and dependent on channel conditions. S-Peak eliminates the dependency on channel conditions but is unable to detect the whereabouts of the channel estimation sequence (CE). Thus, a third algorithm: E-Peak is proposed to overcome their shortfalls by eliminating both dependency on channel conditions and detecting the start of CE. An energy accumulation operation precedes d_0 estimation in E-Peak algorithm whereby

$$E_d = C_d C^*_{d-len} + E_{d-1} \tag{3.6}$$

* denotes a conjugate operation. The series of preceding identical polarity *periods* will result in a maximum peak and this index is translated to estimate d_0, i.e.

$$\hat{d} = \max_{\forall d \in \mathbb{Z}}(E_d) + \alpha \tag{3.7}$$

where α is a constant integer to be determined from simulations' averages. Under noiseless conditions, E_d has the following waveforms for one particular channel realization as shown in Figure 3.5 and Figure 3.6 for UWB CM1 and CM2 respectively.

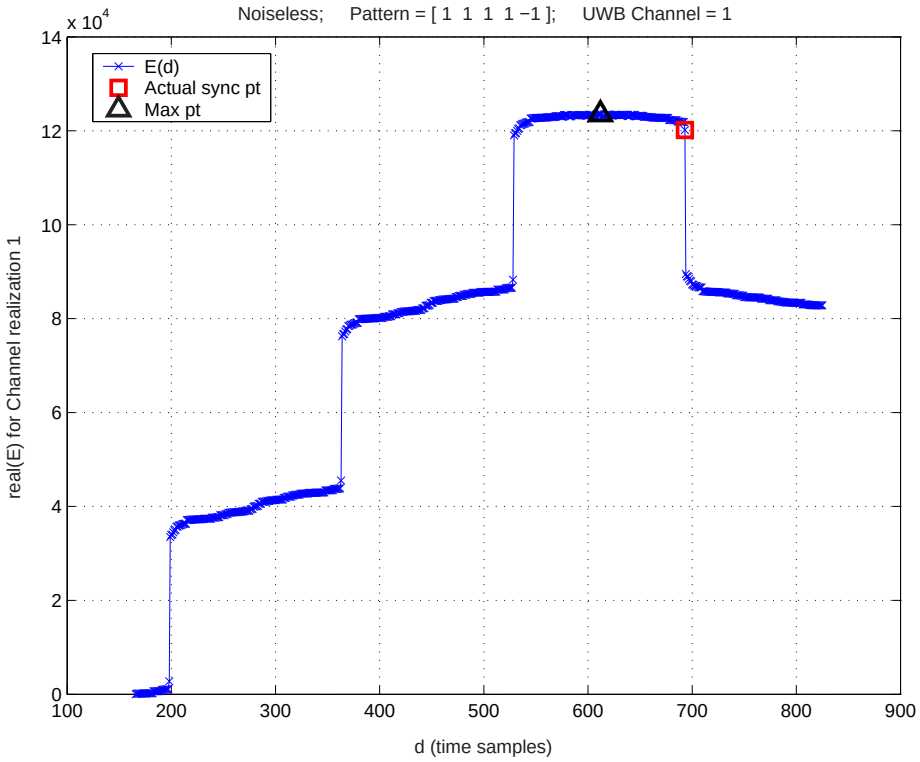

Figure 3.5: E_d for one channel realization under noiseless conditions for UWB CM1

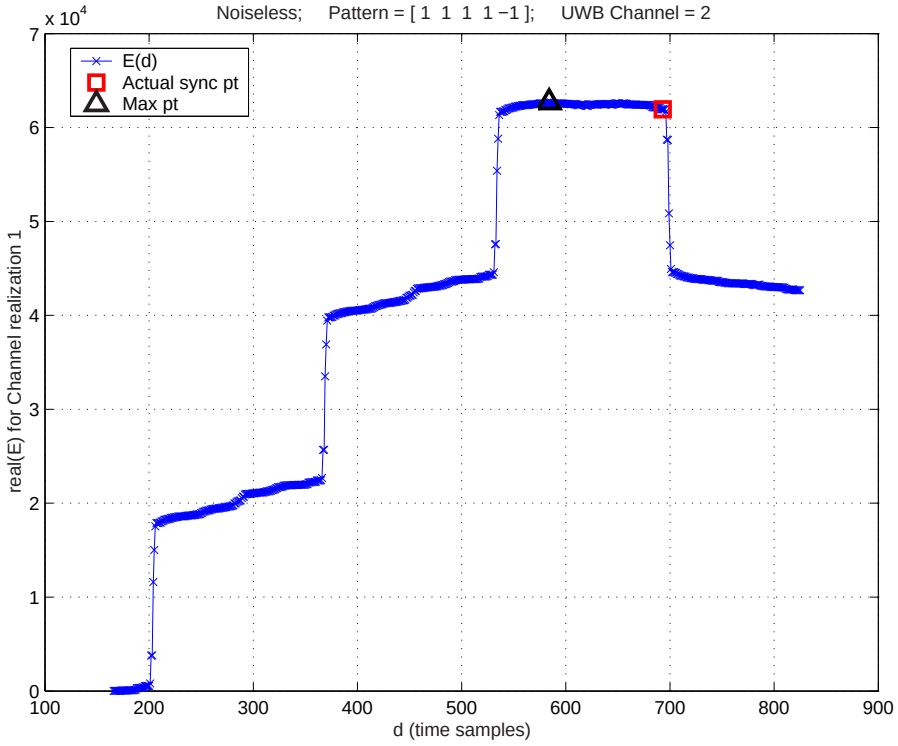

Figure 3.6: E_d for one channel realization under noiseless conditions for UWB CM2

When samples C_d and C_{d-len} are of different polarities, i.e. C_d from FS (-) and C_{d-len} from PS (+), E_d starts to decrease and vice versa, when samples C_d and C_{d-len} are of same polarities, E_d increases. Both increment and decrement is extremely sharp when *pattern* is about aligned with the FFT window of every PS and FS, for example as shown in Figure 3.1. d_0 is estimated then using Equation (3.7).

3.2 Proposed First significant multipath detection via Threshold comparison between Adjacent samples (FTA) algorithm

Using E-Peak, estimating the synchronization point based on correlation results is highly dependent on multipath effects of the UWB channel; a weak first path may cause the receiver to "lock" onto the stronger later paths and synchronize wrongly. Hence the FTA algorithm is proposed to overcome all inadequacies of the other mentioned algorithms. The scheme for FTA synchronization is extended from E-Peak. From Equations (3.1) and (3.2), let

$$\begin{aligned} r_d &= \sum_{i=0}^{l-1} s_{d-i-\theta} h_i + n_d \\ &= y_d + n_d \end{aligned}$$

$$\begin{aligned} \therefore C_d &= \sum_{\substack{k=d \\ m=0}}^{\substack{k=d+N-1 \\ m=N-1}} r_k p_m^* \\ &= \sum_{\substack{k=d \\ m=0}}^{\substack{k=d+N-1 \\ m=N-1}} y_k p_m^* + \underbrace{\sum_{\substack{k=d \\ m=0}}^{\substack{k=d+N-1 \\ m=N-1}} n_k p_m^*}_{w_d} \end{aligned} \tag{3.8}$$

$$
\begin{aligned}
r_{d-len} &= \sum_{i=0}^{l-1} s_{d-len-i-\theta} h_i + n_{d-len} \\
&= y_{d-len} + n_{d-len} \\
\therefore C_{d-len} &= \sum_{\substack{k=d-len \\ m=0}}^{\substack{k=d-len+N-1 \\ m=N-1}} r_k p_m^* \\
&= \sum_{\substack{k=d \\ m=0}}^{\substack{k=d+N-1 \\ m=N-1}} r_{k-len} p_m^* \\
&= \sum_{\substack{k=d \\ m=0}}^{\substack{k=d+N-1 \\ m=N-1}} y_{k-len} p_m^* + \underbrace{\sum_{\substack{k=d \\ m=0}}^{\substack{k=d+N-1 \\ m=N-1}} n_{k-len} p_m^*}_{w_{d-len}}
\end{aligned} \tag{3.9}
$$

Hence,

$$
\begin{aligned}
E_d &= C_d^* C_{d-len} + E_{d-1} \\
&= \Big(\sum_{\substack{k=d \\ m=0}}^{\substack{k=d+N-1 \\ m=N-1}} y_k^* p_m + w_d^* \Big) \Big(\sum_{\substack{k=d \\ m=0}}^{\substack{k=d+N-1 \\ m=N-1}} y_{k-len} p_m^* + w_{d-len} \Big) + E_{d-1} \\
&= \underbrace{\Big(\sum_{\substack{k=d \\ m=0}}^{\substack{k=d+N-1 \\ m=N-1}} y_k^* p_m \Big) \Big(\sum_{\substack{k=d \\ m=0}}^{\substack{k=d+N-1 \\ m=N-1}} y_{k-len} p_m^* \Big)}_{\text{desired user's signal component at } d^{th} \text{ sample}} \\
&\quad + \underbrace{\Big(w_{d-len} \sum_{\substack{k=d \\ m=0}}^{\substack{k=d+N-1 \\ m=N-1}} y_k^* p_m \Big) + \Big(w_d^* \sum_{\substack{k=d \\ m=0}}^{\substack{k=d+N-1 \\ m=N-1}} y_{k-len} p_m^* \Big) + \Big(w_d^* w_{d-len} \Big)}_{\text{noise and other users' interferences}} + E_{d-1}
\end{aligned} \tag{3.10}
$$

Proposed algorithm FTA compares the difference between E_d and E_{d-1} against a pre-determined threshold λ. This difference is represented mathematically in Equation (3.10) above. When the desired user's *pattern* $\vec{p}$ is unaligned with the FFT windows within received signal $\vec{r}$, the desired user's signal component has a small amplitude which cannot be discerned with λ for the correct timing instant d_0. The unwanted noise and other users' interferences are also small after correlation and they form a summing average to zero while the small desired user's signal components are summed up continuously. Hence we should expect E_d to be gradually increasing within the PS *periods*. This scenario accounts for the gentle gradients of plateaus in Figures 3.5 and 3.6.

When the user's *pattern* $\vec{p}$ is almost aligned with each of the FFT windows within $\vec{r}$, the desired user's signal component magnitude increases tremendously and this large magnitude can be detected when it exceeds threshold λ. The focus is on estimating timing point d_0, which is marked by a

large negative magnitude in the desired user's signal component since C_d and C_{d-len} are of opposite polarities. In contrast, the desired user's signal component is a large positive magnitude when C_d and C_{d-len} are of identical polarities. These large magnitudes are depicted also in the same Figures 3.5 and 3.6. Hence, the emphasis is on sieving for a large negative magnitude in the desired user's signal component obtained from $E_d - E_{d-1}$ in Equation (3.10).

The proposed FTA algorithm is summarized in Figure 3.7. When C_d and C_{d-len} belong to *periods* of different polarities, E_d values decrease significantly[1]. The first negative polarity *period* is then deduced to be in this region. A threshold, λ, is used to sieve for the first significant multipath component, exploiting the sharp decrement between E_d and E_{d-1}. The decrement between two consecutive samples, $d-1$ and d, is compared against threshold λ. If the decrement exceeds λ, $\hat{d}$ is deduced to be $d-1$.

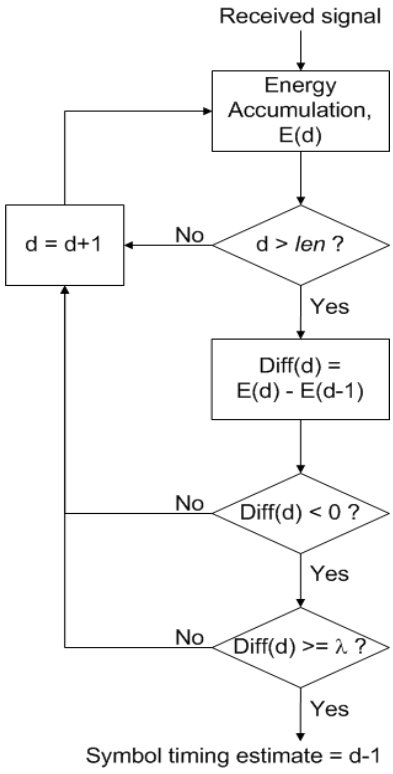

Figure 3.7: Proposed FTA-algorithm timing synchronization scheme

3.3 Timing simulation parameters

The performance of all four synchronization algorithms have been investigated by computer simulation. The OFDM system parameters used are 128 subcarriers IFFT/FFT, together with 32 null

[1]An exception is when E has been computed for less than CP samples since they are affected by noise only

samples pre-appended as CP and 5 null samples appended as G to the 128 length *pattern* $\vec{p}$. Preamble *pattern* 1 is used as the desired user's *pattern* and is given in the Appendix Table 5.1. The corresponding length 6 TFC is $\{1\,3\,2\,1\,3\,2\}$ with a time-domain spreading factor of 2. The number of *periods*, L, considered is 5 for pure timing synchronization. In actual scenarios, L may be fractional but the timing offset θ is assumed to be in units of OFDM samples.

The UWB channel models (CMs) considered are specified by the 802.15.3a channel modeling subcommittee [12]. The typical signal-to-noise ratio (SNR) is 17 dB for UWB CM Line-of-sight (LOS) 0-4m (CM1)and UWB CM Non-line-of-sight (NLOS) 0-4m (CM2). This paper focuses these two CMs.

For E-Peak algorithm, the translation constant α is averaged from noiseless channel realizations to be of value 88 and 79 for CM1 and CM2 respectively. A set of eight threshold values are simulated for FTA synchronization. For each threshold, 100 UWB channels are simulated; under noisy conditions, each of the 100 UWB channels are simulated for 1000 noise realizations., i.e. 100,000 realizations per threshold for each CM.

The signal-to-noise ratio (SNR) is defined as,

$$SNR = \frac{\sigma_s^2}{\sigma_n^2} \tag{3.11}$$

and

$$\sigma_s^2 = \frac{1}{len} \sum_{k=0}^{N-1} |p_k|^2 \tag{3.12}$$

where σ_s^2 is defined as the average transmitted signal power of one preamble subcarrier averaged across one *period*, σ_n^2 is the noise power per subcarrier and $\vec{p} = \{p_0, p_1, \ldots, p_{N-1}\}$ is the transmitted user's preamble *pattern*.

3.4 FTA symbol timing synchronization performance

The mean squared error (MSE) and the total synchronization probability, when considering the safe-zone P_{sync}, are used as performance evaluation criteria.

3.4.1 Mean squared error (MSE)

MSE is defined as:

$$MSE = \sum_{\forall \hat{d}} (\hat{d} - d_0)^2 P(\hat{d})$$

where $P(\hat{d})$ is the probability of synchronization at $\hat{d}$ for the simulated channel realizations. The MSEs for FTA algorithm are summarized as shown in Tables 3.1 and Table 3.2. Based on Table 3.1,the optimum threshold for a typical SNR of 17 dB in UWB CM1 is $\lambda_{optimum} = -21$ dB. Based on Table 3.2,the optimum threshold for a typical SNR of 17 dB in UWB CM2 is $\lambda_{optimum} = -18$ dB.

Table 3.1: Mean squared errors (MSEs) for various thresholds λ dB under UWB CM1: LOS 0-4m for FTA timing synchronization

λ (dB)	SNR (dB)	
for $L = 5$	Noiseless	17
-18	0.510	0.525
-19	0.380	0.410
-20	0.380	0.378
-21	0.380	0.365◀
-22	0.320◀	25.392
-23	0.350	128.600
-24	2.560	483.590
-25	19.940	1523.600

Table 3.2: MSE for various thresholds λ dB under UWB CM2: NLOS 0-4m for FTA timing synchronization

λ (dB)	SNR (dB)	
for $L = 5$	Noiseless	17
-18	9.30	9.129◀
-22	5.26	189.06
-23	4.79	482.55
-24	4.02◀	909.91
-25	5.3	1426
-26	441.15	2331.4
-27	837.41	3984.6
-28	2272.5	7190
-29	4950.3	11586

A large difference between the optimum thresholds of $\lambda = -24$ dB for noiseless and $\lambda = -18$ dB for SNR=17 dB manifests in CM2 (as compared to that of CM1) using the MSE criterion. This implies that the optimum threshold for CM2 is more strongly influenced by SNR as compared to that under CM1. This is a logical observation since CM2 has worse channel conditions without LOS.

Comparing across all the four synchronization algorithms as seen in Tables 3.3 and 3.4, FTA algorithm gives the best performance in terms of MSE as it is at least 75% more accurate than the next best algorithm (S-Peak). In cases of lower SNR, other thresholds can be chosen again suitably to minimise MSE.

Table 3.3: MSE L=5 for various synchronization algorithms for UWB CM1: LOS 0-4m

MSE	SNR (dB)	
	Noiseless	17
FTA	0.380	0.365
E-Peak	421.38	619.19
S-Peak	7.41	7.3102
N-Peak	1.75e5	1.01e5

Table 3.4: MSE L=5 for various synchronization algorithms for UWB CM2: NLOS 0-4m

MSE	SNR (dB)	
	Noiseless	17
FTA	4.02	9.129
E-Peak	561.2	646.31
S-Peak	37.25	37.3632
N-Peak	2.09e5	1.18e5

3.4.2 Probability of synchronization (P_{sync}) with a safe-zone

The safe-zone is defined as the ISI free region of the CP. If $\hat{d}$ falls in the safe-zone, subcarriers will experience phase shifts. If $\hat{d}$ falls outside this zone, subcarriers will experience ISI as well as phase rotations. The influence of ISI is more detrimental to channel estimation and essentially bit error rate (BER) performance of the system. Hence if $\hat{d}$ falls within the safe-zone, timing synchronization is still considered to be achieved. Defining:

$$P_{sync} = P_{sz} + P_{d_0}$$

where P_{sz} is the probability of $\hat{d}$ falling within the safe-zone and P_{d_0} is the probability of estimating $\hat{d} = d_0$, P_{sync} is evaluated for all algorithms and both CMs. For UWB CM1, the maximum delay spread is estimated to be 7 OFDM sample units; hence there is a safe-zone of 25 sample units. For UWB CM2, it is estimated to be 14 sample units; the safe-zone is thus 18 sample units.

Comparing across all the four timing synchronization algorithms, for UWB CM 1, FTA algorithm with $\lambda_{optimum} = -24$ dB outperforms the others with the maximum P_{sync} for SNR = 17 dB environment. The proposed FTA algorithm is at least 53% more likely to achieve timing synchronization compared to the next best algorithm (E-peak). In cases of lower SNR, other thresholds must be chosen again suitably to maximize P_{sync}. For UWB CM 2 under SNR = 17 dB, $\lambda_{optimum} = -27$ dB. In cases of lower SNR, the same performance trend is observed.

Table 3.5: $P_{sync}(\%)$ for various thresholds λ dB under UWB CM1: LOS 0-4m

λ (dB) for $L = 5$	SNR (dB)	
	Noiseless	17
-18	73	72.65
-19	77	76.25
-20	77	77.06
-21	77	77.72
-22	80	79.39
-23	81	80.93
-24	82	81.48◀
-25	85◀	81.22

Table 3.6: $P_{sync}(\%)$ for various thresholds λ dB under UWB channel model 2: NLOS 0-4m

λ (dB) for $L = 5$	SNR (dB)	
	Noiseless	17
-22	31	32.2
-23	36	36
-24	38	39.1
-25	44	45.2
-26	45	47.5
-27	55◀	49.002◀
-28	48	35.658
-29	29	18.183

Table 3.7: $P_{sync}(\%)$ for various algorithms under UWB CM1: LOS 0-4m

$P_{sync}(\%)$	SNR (dB)	
	Noiseless	17
FTA	82	81.48
E-Peak	44	37.603
S-Peak	30	29.926
N-Peak	18	18.19

Table 3.8: $P_{sync}(\%)$ for various algorithms under UWB CM2: NLOS 0-4m

$P_{sync}(\%)$	SNR (dB)	
	Noiseless	17
FTA	55	49.002
E-Peak	21	17.29
S-Peak	3	2.89
N-Peak	1	0.98

From Tables 3.1, 3.2, 3.5 and 3.6 the poor performance of the same threshold in lower SNR environments for both CMs shows that threshold $\lambda_{optimum}$ has to be chosen only after some initial SNR measurements in the desired environment in order to achieve a minimal MSE or high P_{sync}.

The timing synchronization probability distributions of the various algorithms for the noiseless condition under UWB CM1 are presented here for aiding visualization and comparison from Figures 3.8 to 3.11. From these distributions, the MSEs of all algorithms are calculated and tabulated in Tables 3.3, 3.4, 3.7 and 3.8.

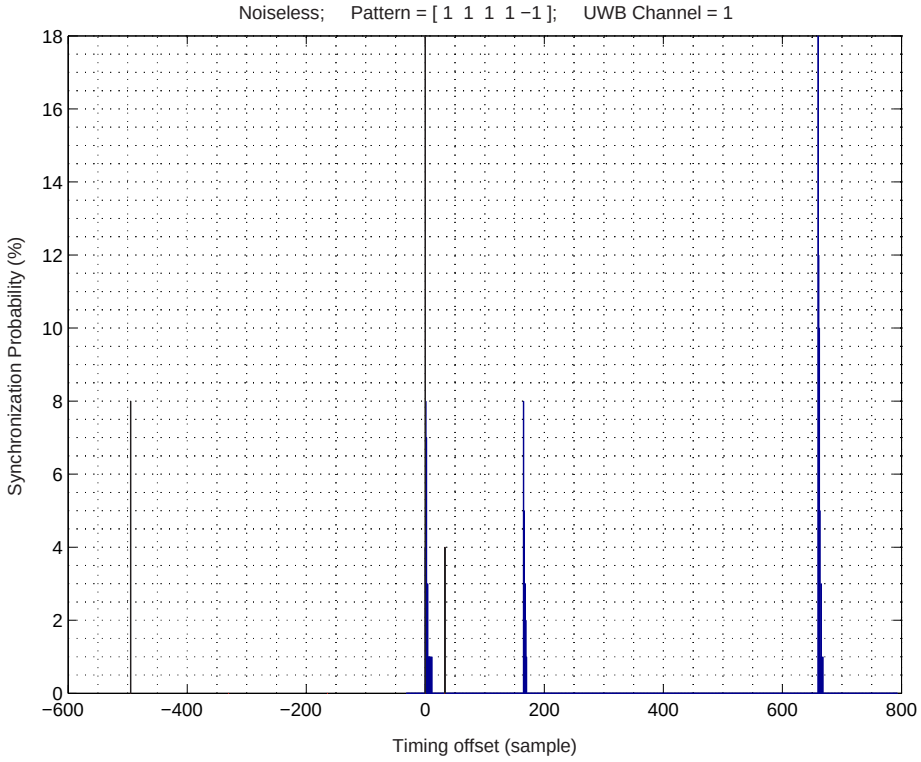

Figure 3.8: Timing synchronization probability distribution using N-Peak under noiseless conditions for UWB CM1 and L=5

In all the MSEs and P_{sync} computations, all 100 UWB channels are considered. For 10% outage, the best 90% channel realizations are retained while the worst 10% channel realizations are discarded. The improved MSE and P_{sync} are as tabulated in Table 3.9 for noiseless cases only with $L = 5$.

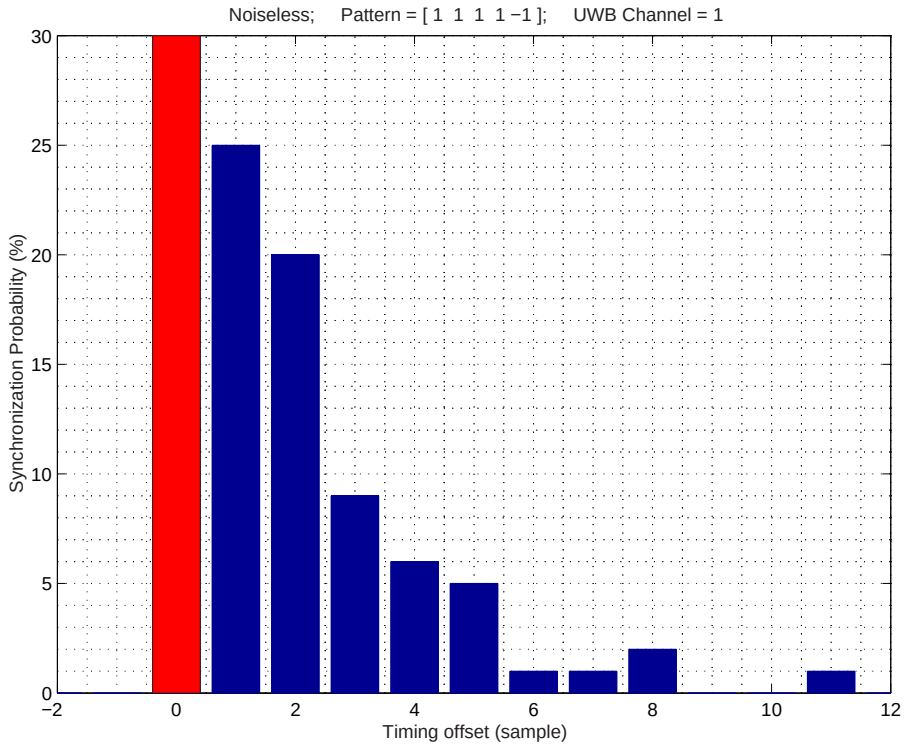

Figure 3.9: Timing synchronization probability distribution using S-Peak under noiseless conditions for UWB CM1 and L=5

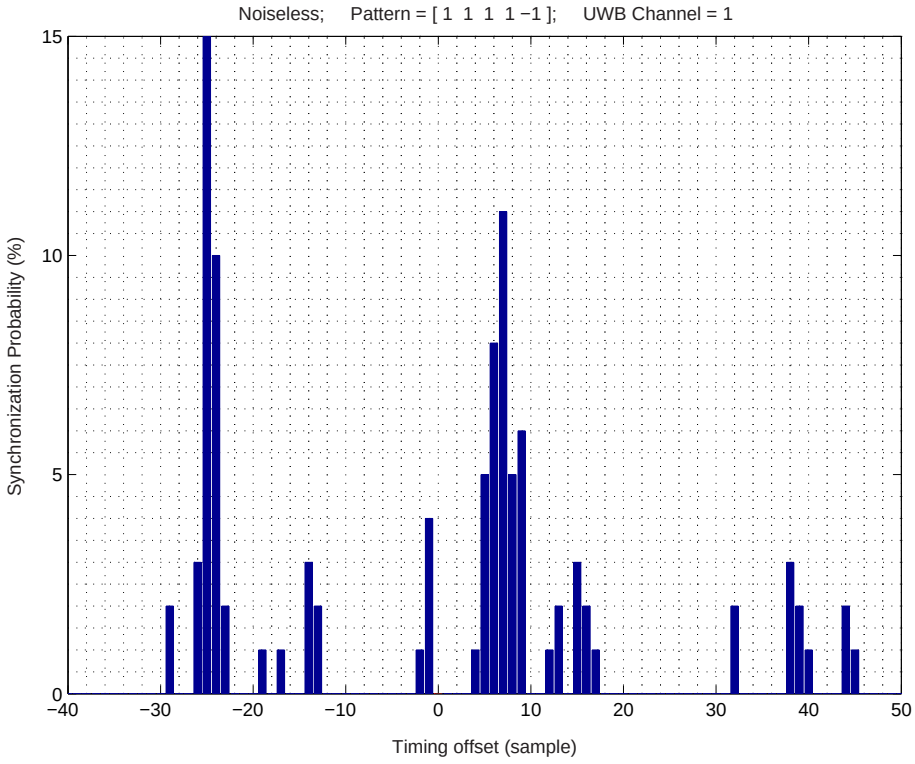

Figure 3.10: Timing synchronization probability distribution using E-Peak under noiseless conditions for UWB CM1 and L=5

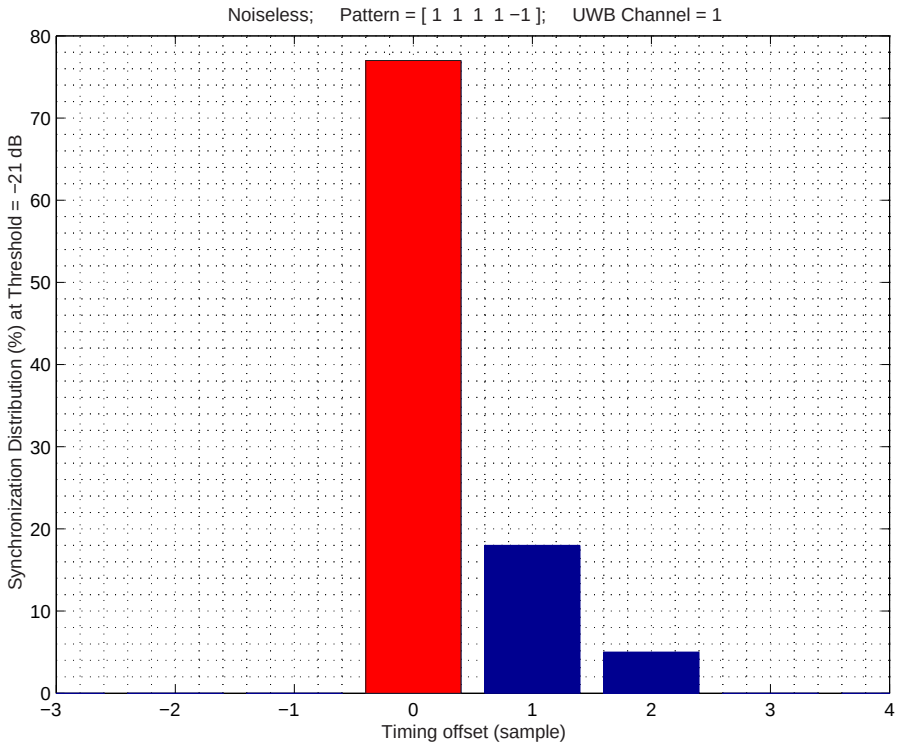

Figure 3.11: Timing synchronization probability distribution using FTA under noiseless conditions for UWB CM1 and L=5

Table 3.9: MSE and $P_{sync}(\%)$ with 10% outage for FTA with $L = 5$ under noiseless conditions

λ(dB)	CM1		λ(dB)	CM2	
	MSE	$P_{sync}(\%)$		MSE	$P_{sync}(\%)$
-18	0.17	81.11	-22	2.36	34.44
-19	0.13	85.56	-23	2.12	40
-20	0.13	85.56	-24	1.86◀	42.22
-21	0.13	85.56	-25	1.68	48.89
-22	0.1◀	88.89	-26	3.31	50
-23	0.13	90	-27	111.88	61.11◀
-24	0.11	91.11	-28	1100.9	53.33
-25	0.82	94.44◀	-29	3729.2	32.22

3.4.3 Robustness of FTA timing synchronization against frequency offset (FO)

In the worst case scenario, signal detection uses up 15 PS *periods*[2] such that only 2 PS and 1 FS *periods* are left for timing and FO estimation. For this case of $L = 3$, FTA timing synchronization probability in the presence of FO is presented.

From Figures 3.12 and 3.13 below, it can be seen that FO has negligible effect on FTA timing synchronization since the timing synchronization distributions remain almost the same with their MSEs as summarized in Table 3.10.

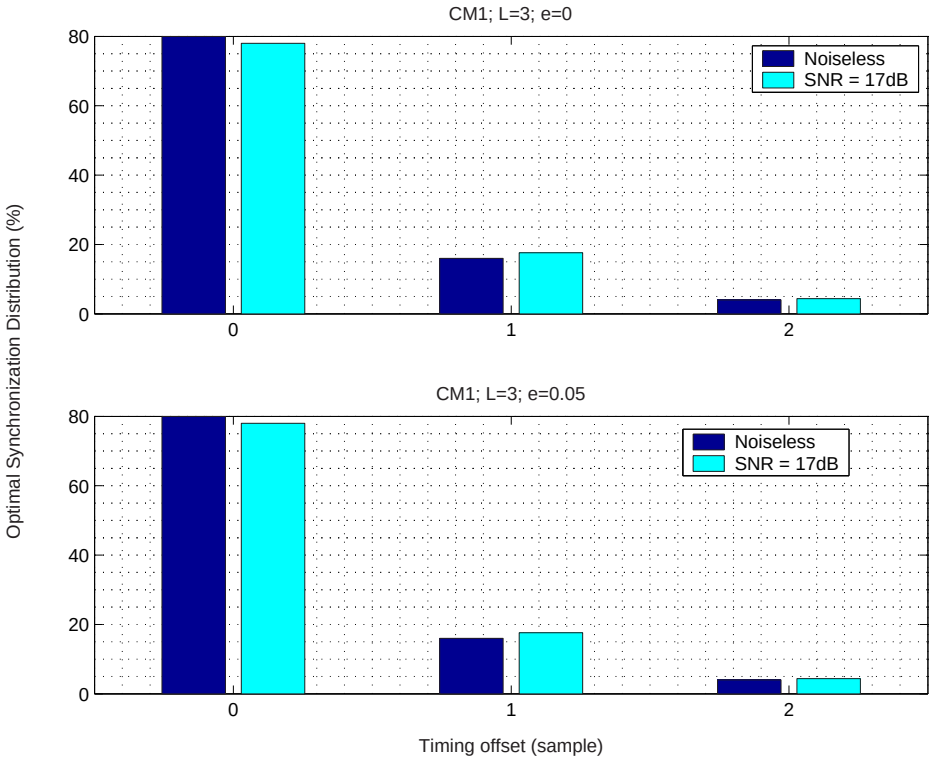

Figure 3.12: FTA timing synchronization probability distribution with no FO versus maximum FO for CM1; MSE=0.371 OFDM samples for $\epsilon = 0.05$ and SNR=17 dB

Table 3.10: Comparison of MSEs with and without FO under SNR=17 dB, $L = 3$ using FTA algorithm

MSE	CM1	CM2
$\epsilon = 0$	0.363	4.569
$\epsilon = 0.05$	0.371	4.548

For practical applications, FO is present and must be considered in timing synchronization. But due to the wideband nature of MB-OFDM, the small FO as compared to intersubcarrier spacing

[2]pCCADetectTime=15 $T_{SYM} = 4.6875\mu$s

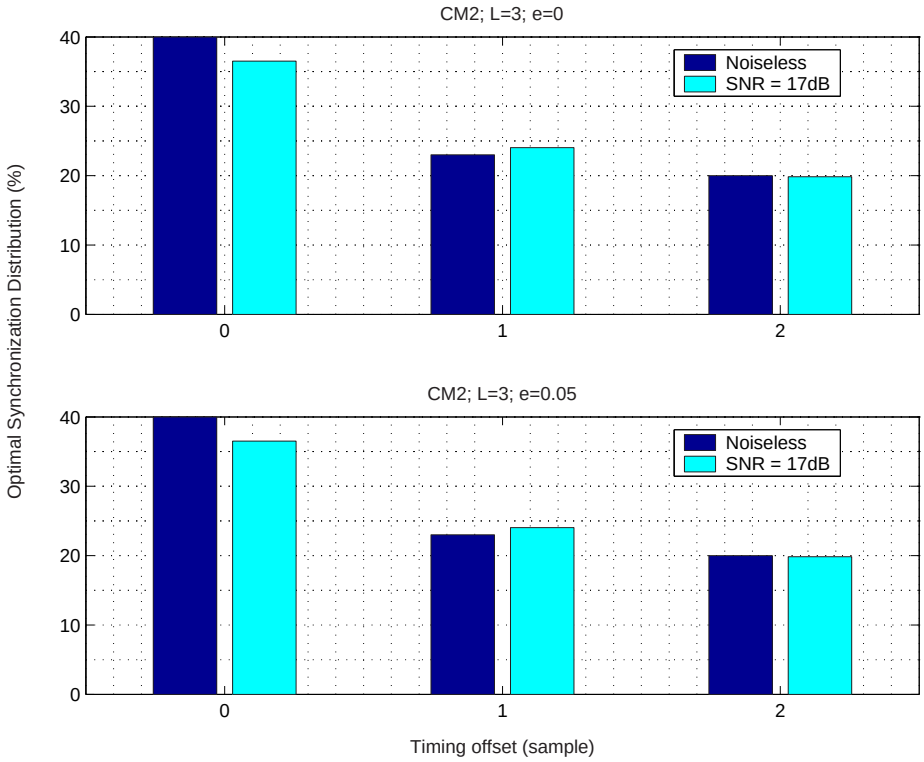

Figure 3.13: FTA timing synchronization probability distribution with no FO versus maximum FO for CM2; MSE=4.548 OFDM samples for $\epsilon = 0.05$ and SNR=17 dB

poses negligible effect.

3.5 Conclusions

Three correlation based algorithms: N-Peak, S-Peak and E-Peak which are extended from conventional OFDM systems, are compared against the proposed algorithm FTA. FTA locks onto the timing estimate when the difference between two consecutive energy samples exceeds a pre-determined threshold. In contrast, other algorithms falsely "lock" onto the strongest MPC through correlation peak and peak energy detection. For $L = 5$, FTA is at least 75% more accurate than the next best algorithm, S-Peak, in terms of mean squared error (MSE) and at least 53% more likely than E-Peak to achieve timing synchronization in terms of synchronization probability (P_{sync}) under a typical operating signal-to-noise ratio (SNR) of 17 dB for both UWB CM1 and CM2. With 10% outage permissible, P_{sync} and MSE performances can be further improved. These are presented in [15]. Further, the robustness of FTA timing synchronization against frequency offset (FO) is also examined and FO is found to have negligible effect on FTA timing synchronization for the multi-band orthogonal frequency division multiplexing (MB-OFDM) UWB system.

Chapter 4

FREQUENCY OFFSET ESTIMATION

4.1 Overview of proposed FTA frequency offset (FO) estimation algorithm

Usually, the frequency offset (FO) estimation problem is approached by separately estimating the integer and and fractional portions. The integer FO presents a phase ambiguity. However, UWB MB-OFDM is designed to have much larger inter-subcarrier frequency spacing when compared to conventional 802.11a/b/g OFDM standards. Hence, the probability of FO being as large or larger than this inter-subcarrier frequency spacing is extremely low for the given system specifications and applications. The problem of estimating the integer portion or any phase ambiguity is therefore eliminated. The phases of accumulated multipath component (MPC) signal strengths in metric E_d from Equation (3.10) in Section 3.2 (page 20) are exploited for estimating the FO.

Let the discrete time domain signal component from Equation (2.4) be represented by y_d. Correspondingly, let its Fourier transform be represented by Y_f. Using Fourier transform properties,

$$Y_{f-f_o} \quad \underrightarrow{IFFT} \quad y_d e^{j2\pi f_o t}$$

where f_o is the actual frequency offset in Hz. Let T_{FFT} denote one preamble *pattern* duration in seconds. In discrete time domain, $t = d \times T_{FFT}/N$ results in

$$Y_{f-f_o} \quad \underrightarrow{IFFT} \quad y_d e^{\frac{j2\pi\epsilon d}{N}}$$

with ϵ denoting the normalized FO with respect to $\Delta_f = 1/T_{FFT}$. Hence it can be seen that FO in the frequency domain manifests as a phase in the time domain. In the presence of timing and frequency offsets, the actual received signal is:

$$\begin{aligned} r_d &= \sum_{i=0}^{l-1} s_{d-i-\theta} h_i e^{\frac{j2\pi\epsilon d}{N}} + n_d \\ &= y_{d-\theta} e^{\frac{j2\pi\epsilon d}{N}} + n_d \end{aligned} \tag{4.1}$$

where l is the channel length, $\otimes$ denotes the convolution operation and n_d denotes a complex AWGN random variable with zero mean and variance σ_n^2. Again, θ denotes the timing offset as in Equation (2.2) in Section 2.4 (page 10) with respect to the first sample, d_0, of the FFT window for the first negative polarity *period* FS. θ has units in terms of OFDM time samples.

The maximum likelihood (ML) FO estimator and Cramer Räo Bound (CRB) are derived in the following Sections 4.2 and 4.3 to serve as benchmarks for the FTA FO estimator variance.

4.2 Maximum likelihood (ML) frequency offset (FO) estimate

Denoting the ML estimate by ϵ_{ML}, the following preliminaries based on the MB-OFDM system are used to derive it, as presented in [16]. The technique to derive the ϵ_{ML} is similar to that in the appendix of [3], with the difference that [3] compared the phases of repeated data symbols for frequency selective Rayleigh fading channels whereas the phases of preamble sequences for the UWB channel are considered here.

$$s_{d-len} = s_d \tag{4.2}$$

$$\begin{aligned} r_d &= (s_d \otimes h_d) e^{\frac{j2\pi\epsilon d}{N}} + n_d \\ &= \sum_{i=0}^{l-1} s_{d-i} h_i e^{\frac{j2\pi\epsilon d}{N}} + n_d \\ &= y_d e^{\frac{j2\pi\epsilon d}{N}} + n_d \end{aligned} \tag{4.3}$$

$$\begin{aligned} r_{d-len} &= \sum_{i=0}^{l-1} s_{d-len-i} h_i e^{\frac{j2\pi\epsilon(d-len)}{N}} + n_{d-len} \\ &= \sum_{i=0}^{l-1} s_{d-i} h_i e^{\frac{j2\pi\epsilon(d-len)}{N}} + n_{d-len} \\ &= y_d e^{\frac{j2\pi\epsilon d}{N}} e^{j\Delta} + n_{d-len} \end{aligned} \tag{4.4}$$

$$\Delta = \frac{-2\pi\epsilon len}{N} \tag{4.5}$$

$$E[r_d] = y_d \tag{4.6}$$

$$E[r_{d-len}] = y_d e^{j\Delta} \tag{4.7}$$

$$E[|r_d|^2] = E[|y_d|^2] + E[|n_d|^2] = \sigma_s^2 + \sigma_n^2 \tag{4.8}$$

$$E[|r_{d-len}|^2] = \sigma_s^2 + \sigma_n^2 \tag{4.9}$$

$$\begin{aligned} r_d r_{d-len}^* &= |y_d|^2 e^{-j\Delta} + y_d n_{d-len}^* + y_d^* n_d e^{-j\Delta} + n_d n_{d-len}^* \\ E[r_d r_{d-len}^*] &= E[|y_d|^2] e^{-j\Delta} = \sigma_s^2 e^{-j\Delta} \end{aligned} \tag{4.10}$$

$$\begin{aligned} r_d^* r_{d-len} &= |y_d|^2 e^{j\Delta} + y_d^* n_{d-len} + y_d n_d^* e^{j\Delta} + n_d^* n_{d-len} \\ E[r_d^* r_{d-len}] &= E[|y_d|^2] e^{j\Delta} = \sigma_s^2 e^{j\Delta} \end{aligned} \tag{4.11}$$

We want to find ϵ_{ML} which maximizes the conditional joint density function of the observations r_d and r_{d-len} for an observation window of length $2len$ samples in $\vec{r}$ within PS *periods* given $\hat{d}$, the estimated timing instant of d_0, from prior timing synchronization. Let d_{upp} and d_{low} denote the

upper and lower limits respectively.

$$d_{upp} = \hat{d} - (L-3)len - 1 \tag{4.12}$$

$$d_{low} = \hat{d} - (L-2)len \tag{4.13}$$

Using Bayes theorem:

$$\begin{aligned}
\epsilon_{ML} &= \max_{\epsilon} \Big[\prod_{d=d_{low}}^{d=d_{upp}} f(\epsilon | r_d, r_{d-len}) \Big] \\
&= \max_{\epsilon} \Big[\prod_{d=d_{low}}^{d=d_{upp}} \frac{f(r_d, r_{d-len}|\epsilon) f(\epsilon)}{f(r_d, r_{d-len})} \Big] \\
&= \max_{\epsilon} \Big[\prod_{d=d_{low}}^{d=d_{upp}} f(r_d, r_{d-len}|\epsilon) \Big] \\
&= \max_{\epsilon} \Big[\prod_{d=d_{low}}^{d=d_{upp}} f\Big(r_d | r_{d-len}, \epsilon\Big) f(r_{d-len}|\epsilon) \Big] \\
&= \max_{\epsilon} \Big[\prod_{d=d_{low}}^{d=d_{upp}} f\Big(r_d | \epsilon, r_{d-len}\Big) \Big]
\end{aligned} \tag{4.14}$$

since known ϵ gives no information about $f(r_{d-len})$, hence

$$f(r_{d-len}|\epsilon) = f(r_{d-len}) \tag{4.15}$$

Density function $f(\epsilon)$ is uniformly distributed whereas $f(r_{d-len})$ and $f(r_d, r_{d-len})$ are independent of ϵ, thus they need not be considered in the maximization. To find the conditional density function in Equation (4.14),

$$\begin{aligned}
r_d &= y_d + n_d \\
&= (r_{d-len} - n_{d-len}) e^{-j\Delta} + n_d \\
&= \underbrace{r_{d-len} e^{-j\Delta}}_{\text{known}} - n_{d-len} e^{-j\Delta} + n_d
\end{aligned} \tag{4.16}$$

$$\therefore E[r_d] = r_{d-len}e^{-j\Delta} \tag{4.17}$$

$$\begin{aligned}\therefore Var[r_d] &= Var[-n_{d-len}e^{-j\Delta} + n_d] \\ &= E[(n_{d-len}e^{-j\Delta} - n_d)(n^*_{d-len}e^{j\Delta} - n^*_d)] \\ &= E[|n_{d-len}|^2] + E[|n_d|^2] \\ &= 2\sigma_n^2 \end{aligned} \tag{4.18}$$

Complex random variable r_d has a Gaussian density function with mean $r_{d-len}e^{-j\Delta}$ and variance $2\sigma_n^2$ given observation r_{d-len} and ϵ. Real and imaginary parts are assumed to be independent.

$$r_{d+len}|\epsilon, r_d = u + jv \tag{4.19}$$

$$u \sim N(\bar{u}, \sigma_n^2) \tag{4.20}$$

$$v \sim N(\bar{v}, \sigma_n^2) \tag{4.21}$$

$$\begin{aligned}\therefore f(r_d|\epsilon, r_{d-len}) &= \frac{1}{\sqrt{2\pi\sigma_n^2}} exp\Big\{\frac{-(u-\bar{u})^2}{2\sigma_n^2}\Big\} \times \frac{1}{\sqrt{2\pi\sigma_n^2}} exp\Big\{\frac{-(v-\bar{v})^2}{2\sigma_n^2}\Big\} \\ &= \frac{1}{2\pi\sigma_n^2} exp\Big\{\frac{-[(u-\bar{u})^2 + (v-\bar{v})^2]}{2\sigma_n^2}\Big\} \\ &= \frac{1}{2\pi\sigma_n^2} exp\Big\{\frac{-|r_d - r_{d-len}e^{-j\Delta}|^2}{2\sigma_n^2}\Big\} \\ &= \frac{1}{2\pi\sigma_n^2} exp\Big\{\frac{-(r_d - r_{d-len}e^{-j\Delta})(r_d - r_{d-len}e^{-j\Delta})^*}{2\sigma_n^2}\Big\} \end{aligned} \tag{4.22}$$

$$\therefore f(r_d|\epsilon, r_{d-len}) = \frac{1}{2\pi\sigma_n^2} exp\Big\{\frac{-(r_d - r_{d-len}e^{-j\Delta})(r_d - r_{d-len}e^{-j\Delta})^*}{2\sigma_n^2}\Big\} \tag{4.23}$$

Substituting Equation (4.23) in Equation (4.14),

$$\begin{aligned}
\epsilon_{ML} &= \max_{\epsilon} \Big[\prod_{d=d_{low}}^{d=d_{upp}} f\Big(r_d|\epsilon, r_{d-len}\Big)\Big] \\
&= \max_{\epsilon} \Big[\prod_{d=d_{low}}^{d=d_{upp}} \frac{1}{2\pi\sigma_n^2} exp\Big\{ \frac{-(r_d - r_{d-len}e^{-j\Delta})(r_d - r_{d-len}e^{-j\Delta})^*}{2\sigma_n^2} \Big\}\Big] \\
&= \max_{\epsilon} \Big[\sum_{d=d_{low}}^{d=d_{upp}} \ln\Big(\frac{1}{2\pi\sigma_n^2} exp\Big\{ \frac{-(r_d - r_{d-len}e^{-j\Delta})(r_d - r_{d-len}e^{-j\Delta})^*}{2\sigma_n^2} \Big\}\Big)\Big] \\
&= \max_{\epsilon} \Big[\sum_{d=d_{low}}^{d=d_{upp}} \Big\{ \ln \frac{1}{2\pi\sigma_n^2} + \frac{-(r_d - r_{d-len}e^{-j\Delta})(r_d - r_{d-len}e^{-j\Delta})^*}{2\sigma_n^2} \Big\}\Big] \\
&= \min_{\epsilon} \Big[\sum_{d=d_{low}}^{d=d_{upp}} (r_d - r_{d-len}e^{-j\Delta})(r_d - r_{d-len}e^{-j\Delta})^* \Big] \\
&= \min_{\epsilon} \Big[\sum_{d=d_{low}}^{d=d_{upp}} \Big(|r_d|^2 - r_d^* r_{d-len} e^{-j\Delta} - r_d r_{d-len}^* e^{j\Delta} + |r_{d-len}|^2 \Big)\Big] \\
&= \max_{\epsilon} \Big[Re\{ \underbrace{\sum_{d=d_{low}}^{d=d_{upp}} r_d r_{d-len}^*}_{\alpha} e^{j\Delta} \} \Big] \\
&= \max_{\epsilon} \Big[|\alpha| \cos\left(\Delta + \angle\alpha\right) \Big]
\end{aligned} \tag{4.24}$$

where $\angle\alpha$ denotes the phase of α. Maxima occurs when the cosine term equals to one. This yields the ML estimate of

$$\begin{aligned}
\Delta + \angle\alpha &= 2\zeta\pi; \quad \zeta = integer \\
\therefore \epsilon_{ML} &= \frac{-\zeta N}{len} + \frac{N\angle\alpha}{2\pi len}
\end{aligned}$$

For MB-OFDM UWB systems, the wide bandwidth allows for less stringent frequency synchronization requirements. The transmitter and receiver oscillators are specified to have a maximum frequency tolerance of ± 20 ppm[1]. Consider the mandatory Mode 1 bands, as shown in Figure 4.2. The highest frequency band has a center frequency of 4488 MHz. The maximum FO possible resulting from mismatched transmitter and receiver oscillators evaluates to

$$\begin{aligned}
f_0 &= 40ppm \times f_c \\
&= \frac{40}{1,000,000} \times 4488 \times 10^6 \\
&= 179.52kHz
\end{aligned} \tag{4.25}$$

[1] parts per million

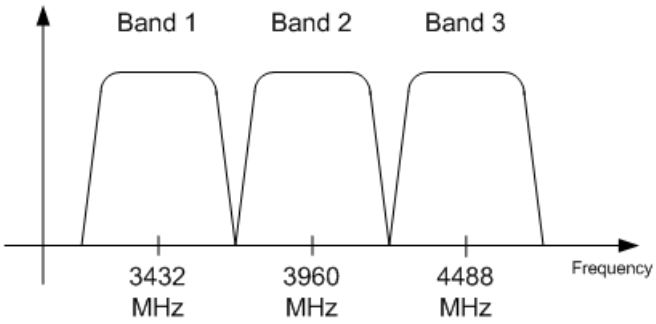

Figure 4.1: Frequency of operation for a Mode 1 device

where f_c is the center frequency of Band 3 for Mode 1 operation.

$$\epsilon_{max} = \frac{f_0}{\Delta_f} = \frac{179.52kHz}{4.125MHz} = 0.04352 \tag{4.26}$$

Hence the FO results in only fractional offsets as show in Equation (4.26) and eliminates the need to resolve the integer ambiguity portion . For high data rate applications, mobility is limited translating to small Doppler spreads. Since $|\epsilon| << 1$, thus it can be safe to say that $\zeta = 0$

$$\therefore \epsilon_{ML} = \frac{N\angle\alpha}{2\pi len} = \frac{N}{2\pi len}\angle\Big(\sum_{d=d_{low}}^{d=d_{upp}} r_d r^*_{d-len}\Big) \tag{4.27}$$

4.3 Cramer Räo Bound (CRB)

Let $\Lambda(\epsilon)$ denote the log-likelihood function from which the CRB is derived for the MB-OFDM system. This derivation is also presented in [16].

$$\begin{aligned}
\Lambda(\epsilon) &= \ln\Big[\prod_{d=d_{low}}^{d=d_{upp}} f(r_d|\epsilon, r_{d-len})\Big] \\
&= \sum_{d=d_{low}}^{d=d_{upp}} \Big[\ln f(r_d|\epsilon, r_{d-len})\Big] \\
&= \sum_{d=d_{low}}^{d=d_{upp}} \Big[\ln\frac{1}{2\pi\sigma_n^2} - \frac{1}{2\sigma_n^2}(r_d - r_{d-len}e^{-j\Delta})(r_d - r_{d-len}e^{-j\Delta})^*\Big] \\
&= \sum_{d=d_{low}}^{d=d_{upp}} \Big[\ln\frac{1}{2\pi\sigma_n^2} - \frac{1}{2\sigma_n^2}\Big(|r_d|^2 - r_d^* r_{d-len}e^{-j\Delta} - r_d r^*_{d-len}e^{j\Delta} + |r_{d-len}|^2\Big)\Big] \\
&= \sum_{d=d_{low}}^{d=d_{upp}} \Big[\ln\frac{1}{2\pi\sigma_n^2} - \frac{1}{2\sigma_n^2}\Big(|r_d|^2 - 2Re(\underbrace{r_d r^*_{d-len}}_{\beta}e^{j\Delta}) + |r_{d-len}|^2\Big)\Big] \\
&= \sum_{d=d_{low}}^{d=d_{upp}} \Big[\ln\frac{1}{2\pi\sigma_n^2} - \frac{1}{2\sigma_n^2}\Big(|r_d|^2 - 2|\beta|\cos(\Delta + \angle\beta) + |r_{d-len}|^2\Big)\Big]
\end{aligned} \tag{4.28}$$

Hence, from [17] and [18], taking the first and second order partial derivatives yield:

$$\begin{aligned}\therefore \frac{d\Lambda(\epsilon)}{d\epsilon} &= \frac{1}{\sigma_n^2}\sum_{d=d_{low}}^{d=d_{upp}} \frac{d}{d\epsilon}\Big\{|\beta|\cos(\Delta+\angle\beta)\Big\} \\ &= \frac{-1}{\sigma_n^2}\sum_{d=d_{low}}^{d=d_{upp}} |\beta|\sin(\Delta+\angle\beta)\Big(\frac{2\pi len}{N}\Big) \end{aligned} \tag{4.29}$$

$$\therefore \frac{d^2\Lambda(\epsilon)}{d\epsilon^2} = \frac{-1}{\sigma_n^2}\sum_{d=d_{low}}^{d=d_{upp}} |\beta|\cos(\Delta+\angle\beta)\Big(\frac{2\pi len}{N}\Big)^2 \tag{4.30}$$

Denoting the Fisher information as J,

$$\begin{aligned}\therefore J &= -E\Big[\frac{d^2\Lambda(\epsilon)}{d\epsilon^2}\Big] \\ &= \frac{4\pi^2 len^2}{N^2\sigma_n^2}\sum_{d=d_{low}}^{d=d_{upp}} E\Big[|\beta|\cos(\Delta+\angle\beta)\Big] \\ &= \frac{4\pi^2 len^2}{N^2\sigma_n^2}\sum_{d=d_{low}}^{d=d_{upp}} E\Big[|\beta|\cos\Delta\cos\angle\beta - |\beta|\sin\Delta\angle\beta\Big] \\ &= \frac{4\pi^2 len^2}{N^2\sigma_n^2}\sum_{d=d_{low}}^{d=d_{upp}} E\Big[Re(\beta)\cos\Delta - Im(\beta)\sin\Delta)\Big] \\ &= \frac{4\pi^2 len^2}{N^2\sigma_n^2}\sum_{d=d_{low}}^{d=d_{upp}} \Big[\sigma_s^2\cos^2\Delta + \sigma_s^2\sin^2\Delta)\Big] \\ &= \frac{4\pi^2 len^2}{N^2}\frac{\sigma_s^2}{\sigma_n^2}\sum_{d=d_{low}}^{d=d_{upp}} (1) \\ &= \frac{4\pi^2 len^3 SNR}{N^2} \end{aligned} \tag{4.31}$$

where signal-to-noise ratio (SNR) is defined as in Section 3.3 (page 22). Inverting Fisher information J yields the CRB of

$$Var(\hat{\epsilon}) \geq \frac{N^2}{4\pi^2 len^3 SNR} \tag{4.32}$$

Aside,

$$\begin{aligned} E[Re(\beta)] &= Re(E[\beta]) \\ &= Re(E[y_d r_{d-len}^*]) \\ &= Re(E[|y_d|^2]e^{-j\Delta}) \\ &= \sigma_s^2\cos\Delta \end{aligned} \tag{4.33}$$

$$\begin{aligned} E[Im(\beta)] &= Im(E[\beta]) \\ &= Im(E[y_d r^*_{d-len}]) \\ &= Im(E[|y_d|^2]e^{-j\Delta}) \\ &= -\sigma_s^2 \sin\Delta \end{aligned} \tag{4.34}$$

With the ML FO estimator and CRB derived as a basis for comparison, the proposed FTA FO estimator is derived in the following Section.

4.4 Proposed FTA frequency offset (FO) estimator

For the noiseless case, the received signal waveform is represented by

$$r_d = y_d e^{\frac{j2\pi\epsilon d}{N}} \tag{4.35}$$

$$\begin{aligned} r_{d-len} &= y_{d-len} e^{\frac{j2\pi\epsilon(d-len)}{N}} \\ &= r_d e^{\frac{-j2\pi\epsilon len}{N}} \\ &= r_d e^{j\Delta}, \text{with} \quad \Delta = \frac{-2\pi\epsilon len}{N} \end{aligned} \tag{4.36}$$

After correlation with desired user's preamble *pattern* $\vec{p}$,

$$C_d = \sum_{\substack{k=d \\ m=0}}^{\substack{k=d+N-1 \\ m=N-1}} r_k p^*_m \tag{4.37}$$

$$\begin{aligned} C_{d-len} &= \sum_{\substack{k=d-len \\ m=0}}^{\substack{k=d+N-len-1 \\ m=N-1}} r_k p^*_m \\ &= \sum_{\substack{k=d \\ m=0}}^{\substack{k=d+N-1 \\ m=N-1}} r_{k-len} p^*_m \\ &= \sum_{\substack{k=d \\ m=0}}^{\substack{k=d+N-1 \\ m=N-1}} r_k e^{j\Delta} p^*_m \\ &= C_d e^{j\Delta} \end{aligned} \tag{4.38}$$

To obtain the phase for FO estimation, there is a time delay of len samples as $E_{-1}, E_0, E_1, \ldots, E_{len-1} = 0$ due to $C_{-len}, C_{-len+1}, \ldots, C_{-1} = 0$. Hence, recursive Equation (3.6) evaluates to

For $d < len$:

$$\begin{aligned} E_0 &= C_0^* C_{-len} + E_{-1} = 0 \\ E_1 &= C_1^* C_{1-len} + E_0 = 0 \\ &\vdots \\ E_{len-1} &= C_{len-1}^* C_{-1} + E_{len-2} = 0 \end{aligned}$$

For $d \geq len$:

$$\begin{aligned} E_{len} &= C_{len}^* C_0 + E_{len-1} \\ &= C_{len}^* C_{len} e^{j\Delta} \\ &= |C_{len}|^2 e^{j\Delta} \end{aligned}$$

$$\begin{aligned} E_{len+1} &= C_{len+1}^* C_1 + E_{len} \\ &= C_{len+1}^* C_{len+1} e^{j\Delta} + |C_{len}|^2 e^{j\Delta} \\ &= e^{j\Delta}\Big[|C_{len+1}|^2 + |C_{len}|^2\Big] \\ &\vdots \\ E_d &= C_d^* C_{d-len} + E_{d-1} \\ &= e^{j\Delta}\Big[|C_d|^2 + \ldots + |C_{len+1}|^2 + |C_{len}|^2\Big] \end{aligned} \tag{4.39}$$

Therefore, the phase of E_d yields the desired ϵ. Denoting $\angle\gamma$ as the phase of γ,

$$\angle E_d = \Delta = 2\zeta\pi + \Delta_s \tag{4.40}$$

in general where ζ is an integer which is constant for all d and Δ_s denotes the fractional FO. Recall that for UWB MB-OFDM system, ζ can safely be assumed as zero based on Equation (4.26), i.e. $\Delta = \Delta_s$

$$\therefore \hat{\epsilon_d} = \frac{-N\angle E_d}{2\pi len}$$

Considering noise now, an average is taken across N samples of metric E_d. Hence, the final expression for the proposed FTA FO estimator is

$$\hat{\epsilon} = \frac{-1}{2\pi len} \sum_{d=\hat{d}-(L-1)len}^{\hat{d}-(L-1)len+N-1} \angle E_d \tag{4.41}$$

The derivation above for FTA FO estimator is presented in [19]. FTA FO estimator performance is now compared against that of ML estimator and the CRB.

4.5 Frequency offset (FO) estimation simulation parameters

The number of transmitted PS and FS *periods* is $L = 3$. Simulations are carried out for both UWB UWB CM Line-of-sight (LOS) 0-4m (CM1) and UWB CM Non-line-of-sight (NLOS) 0-4m (CM2). All 100 channel realizations for each channel model are as depicted in [12] and each channel iterated for 1000 noisy realizations. Based on Equation (4.26), the maximum normalized FO used in all simulations is set as $\epsilon = 0.05$ and $L = 3$, i.e. $\vec{s} = \{PS, PS, FS, CE, CE\}$.

4.6 FTA frequency offset (FO) estimator performance

The FO estimator performance evaluation criterion is the estimator variance defined by:

$$Var(\hat{\epsilon}) = \frac{1}{CR} \sum_{CR} (\hat{\epsilon} - \bar{\hat{\epsilon}})^2 \tag{4.42}$$

where CR denotes the total number of channel realizations, $\bar{\hat{\epsilon}}$ denotes the mean of estimates $\hat{\epsilon}$ averaged over all CR.

4.6.1 FTA frequency offset (FO) estimator performance against timing offsets

The robustness of Equation (4.41) against timing offset (TO) or θ is shown in Figure 4.2 and Figure 4.3 for CM1 and CM2 respectively. It can be seen that for $L = 3$, the large variance for timing error towards CP is due to the initial E metric samples from Equation (3.6) being composed of noise alone; the low variance for timing offset away from CP is due to noise averaging out as E metric samples are summed up. Hence for $\theta > 0$, FO estimation is still highly accurate.

4.6.2 FTA frequency offset (FO) estimator performance against maximum likelihood (ML) estimator performance and Cramer Räo Bound (CRB)

FTA FO estimation performance is compared against that of maximum likelihood (ML) FO estimation. The ML estimator has been derived as shown in Equation (4.27) under Section 4.2 (pg. 32). Figure 4.4 shows the performances of FTA and ML FO estimators where FTA timing synchronization

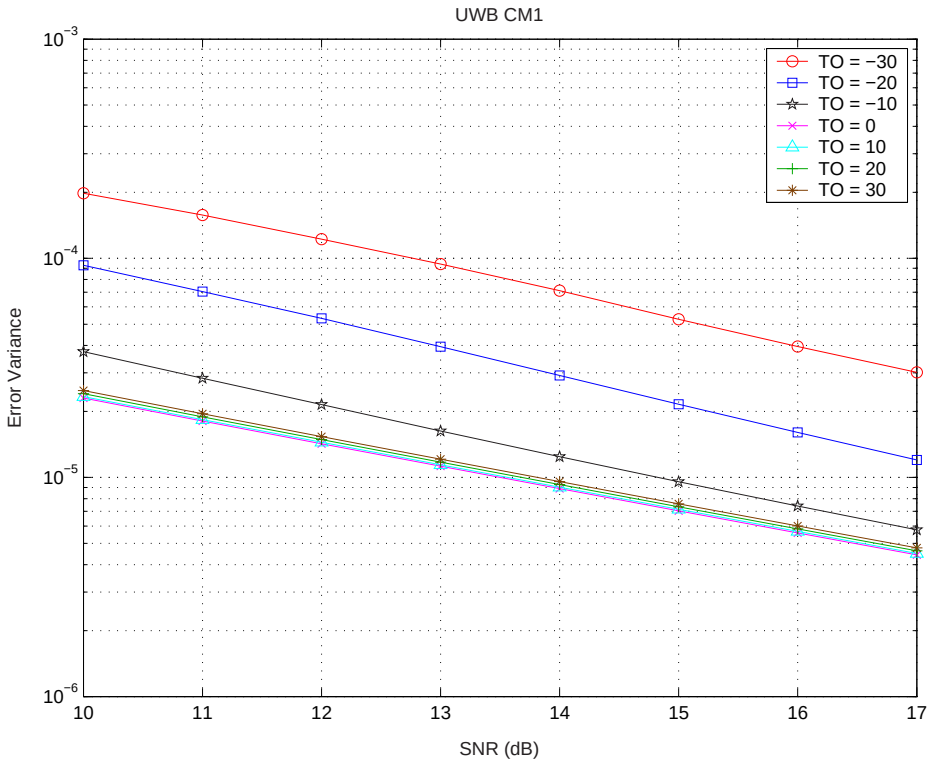

Figure 4.2: Robustness of FTA FO estimation against timing offset (TO) for UWB CM1

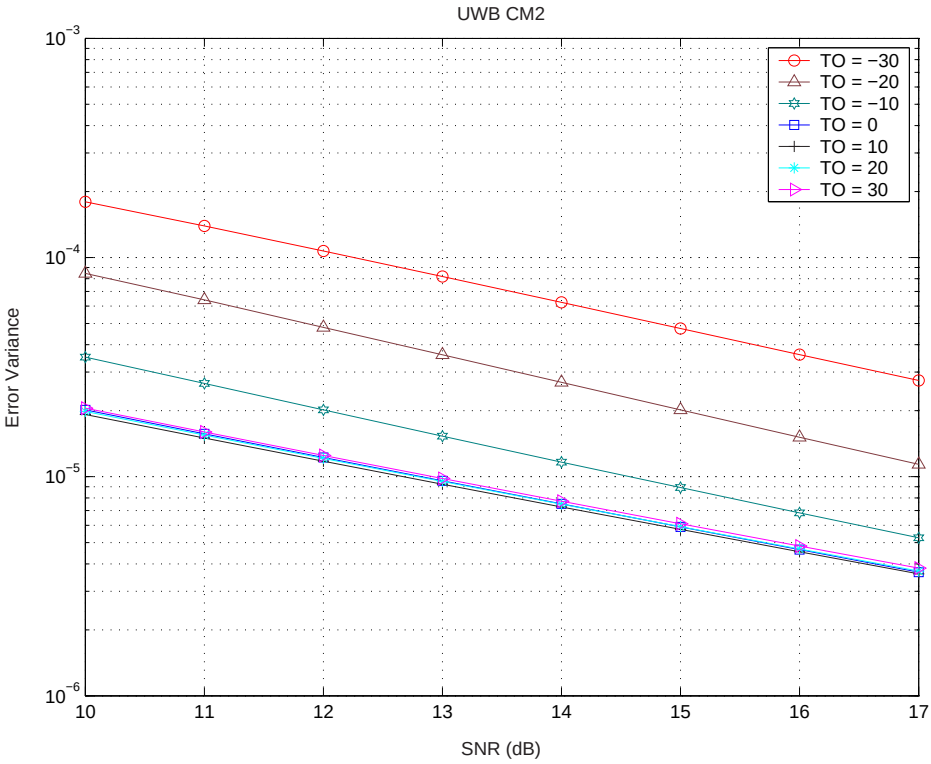

Figure 4.3: Robustness of FTA FO estimation using against timing offset (TO) for UWB CM2

preceded FTA FO estimation and ML estimators are simulated under no timing errors, i.e. $\theta = 0$.

The Cramer Räo Bound (CRB) has been derived as shown in Equation (4.32) under Section 4.3 (pg. 37). Figure 4.5 shows the ML estimator performance against the CRB for a wider SNR range under AWGN channel as well as UWB CM Line-of-sight (LOS) 0-4m (CM1) and UWB CM Non-line-of-sight (NLOS) 0-4m (CM2). Recall from Equation (3.11), the SNR is defined as the average transmitted signal power of one preamble subcarrier averaged across one *period* against noise power per subcarrier. The actual received SNR depends on the channel gain and this is given by:

$$SNR_i = \frac{\sum_{l+N-1} |\vec{h_i} \otimes \vec{p}|^2}{\sigma_n^2 \times len} \tag{4.43}$$

where $\vec{h_i} = \{h_{i0}, h_{i1}, \ldots, h_{i(l-1)}\}$ denotes the i^{th} channel realization and $\otimes$ denotes a convolution operation. Since only 100 UWB channels are evaluated per CM, the channel gain inevitably deviates from unity gain. So a fairer comparison will be that of ML estimator variance against CRB_{avg} where

$$CRB_{avg} = \int \frac{N^2}{4\pi^2 len^3 SNR_i} P(SNR_i) \quad dSNR_i \tag{4.44}$$

$P(SNR_i)$ denotes the probability of a channel realization resulting in SNR_i derived according to Equation (4.43). This is equivalent to receiving a signal with SNR_i at the receiver. The ML FO estimator variance is compared against CRB_{avg} as shown in Figure 4.6. Note that Equation (4.27) is simulated with no timing errors, i.e. $\theta = 0$, and its variance against the CRB is shown in Figure 4.6. Zooming into Figure 4.6, ML estimator variance is seen to converge with CRB_{avg} as shown in Figure 4.7 and this outcome is consistent with that of [18].

4.7 Conclusions

The FTA frequency offset (FO) estimation algorithm is extended from the proposed metric E_d whereby the phase differences between each subcarrier of two adjacent identical training symbols are extracted and averaged to yield the FTA FO estimator. The FTA FO estimator based on Equation (4.41) gives a low variance of 4.118×10^{-6} under SNR of 17 dB for UWB channel model (CM) CM1 and a variance of 3.580×10^{-6} with SNR of 17 dB for UWB CM2. Further, the robustness of FTA FO estimator against timing offset is discussed for both UWB channel models (CMs). When compared against their respective maximum likelihood (ML) estimator variances (no timing errors for ML estimators) for both UWB CMs, FTA FO estimator variances suffered SNR losses of less than 0.5 dB, in each case with FTA timing synchronization preceding FTA FO estimation. Towards the

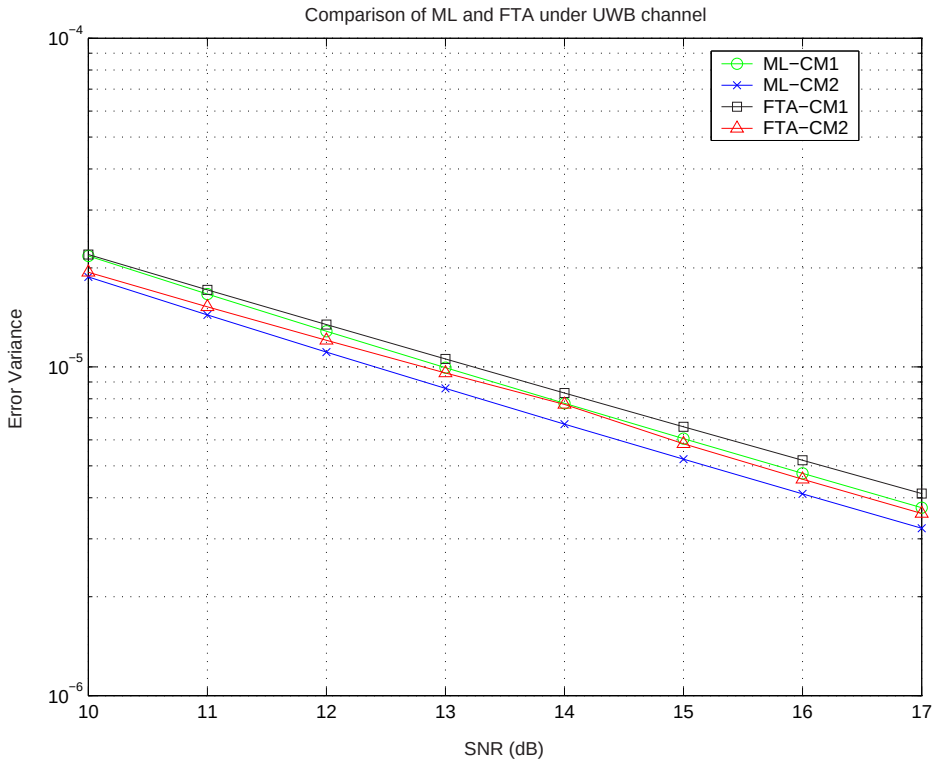

Figure 4.4: Comparison of FTA FO estimator variance with timing errors from prior FTA timing synchronization against ML FO estimator variance with no timing errors

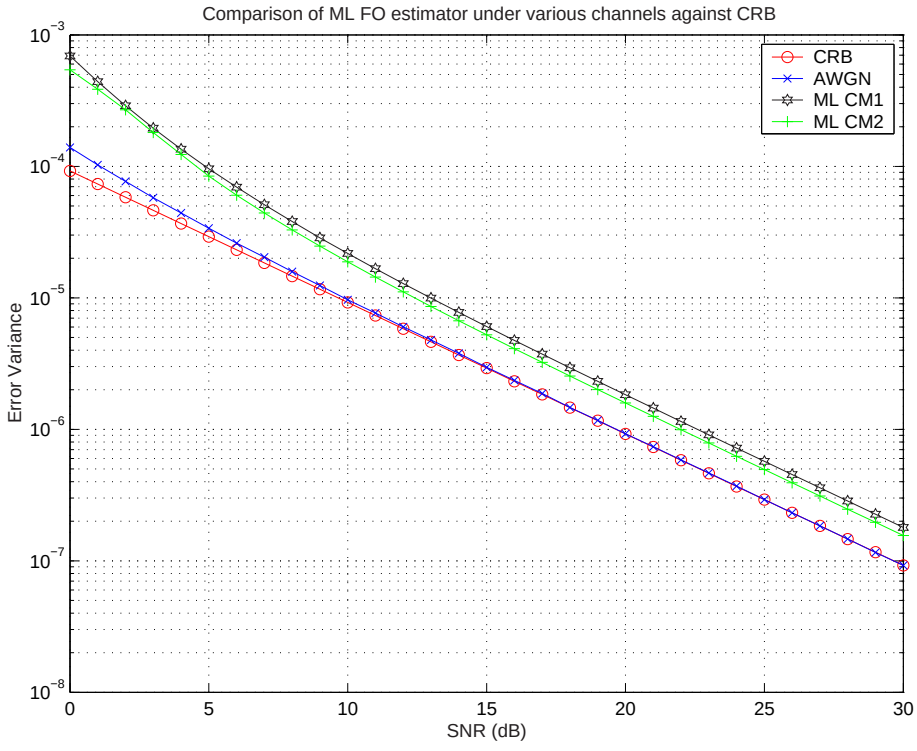

Figure 4.5: Comparison of ML FO estimator performance against CRB

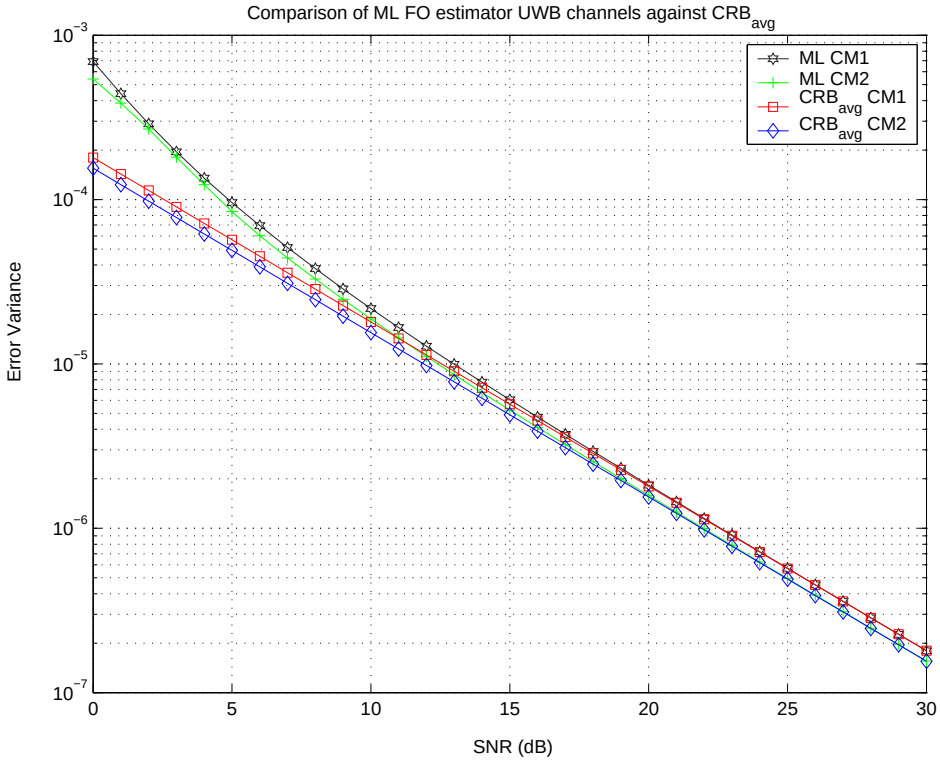

Figure 4.6: Comparison of ML FO estimator performance against CRB_{avg} for 100 UWB channels

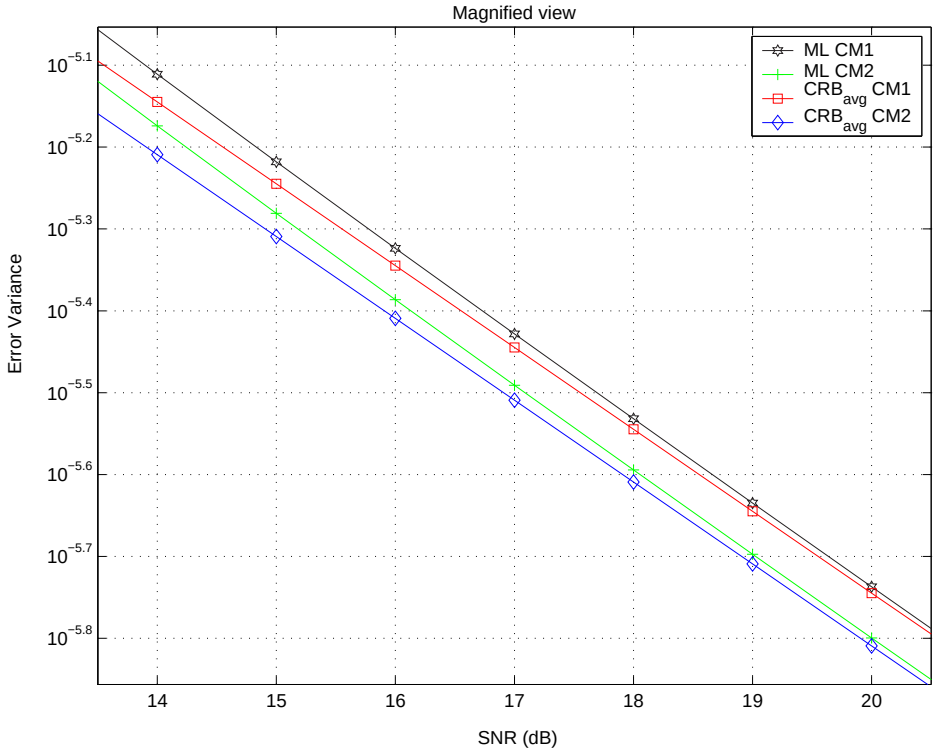

Figure 4.7: Magnified view of ML estimator performance against CRB_{avg} under UWB CM1 and CM2 for high SNR region

high SNR region, ML FO estimator variances converge to their averaged Cramer R*ä*o Bounds (CRBs) defined as per Equation (4.44) which takes into consideration non-unity channel gain.

Chapter 5

CONCLUSIONS

The proposed algorithm First significant multipath detection via Threshold comparison between Adjacent samples (FTA) yields excellent performance for symbol timing synchronization and carrier frequency offset estimation, both of which are critical for accurate channel estimation which follows. FTA makes use of the difference between adjacent accumulated energy samples to compare against an optimum threshold whereby this threshold is determined beforehand by the receiver from measurements of the surrounding's signal-to-noise ratio (SNR). The correct timing instant or FFT window is affirmed when this threshold is crossed. Frequency offset (FO) estimation is then carried out with the obtained timing information by comparing the phase differences between subcarriers of adjacent preamble *periods* having identical polarities. These phase differences from the large number of subcarriers are averaged to obtain a good FO estimate. Timing mean squared errors from FTA are low with UWB CM1 at 0.371 OFDM time samples and CM2 at 4.548 OFDM time samples for the typical operating SNR of 17 dB. Compared to the other conventional OFDM system extended algorithms (N-Peak, S-Peak and E-Peak), the proposed FTA algorithm is at least 75% more accurate than the next best algorithm in terms of MSE and at least 53% more likely to achieve timing synchronization in terms of synchronization probability. The FTA frequency offset estimator variances under the same SNR are in orders of 10^{-6} for both UWB channel models. Compared against the maximum likelihood estimator variances and the averaged Cramer R*äo* Bounds, the FTA estimator variances suffered a SNR loss of less than 0.5 dB with timing information obtained using FTA timing synchronization algorithm. The robustness of FTA timing synchronization against frequency offset (FO) and that of FTA FO estimation versus timing offset is also discussed. FO is found to have negligible effects on FTA timing synchronization performance while FTA FO estimator still gives good performance in the event of timing offset.

Appendix

Table 5.1: Time-domain Preamble Pattern 1

Sequence Element	Value	Sequence Element	Value	Sequence Element	Value	Sequence Element	Value
p_0	0.6564	p_{32}	-0.0844	p_{64}	-0.2095	p_{96}	0.4232
p_1	-1.3671	p_{33}	1.1974	p_{65}	1.1640	p_{97}	-1.2684
p_2	-0.9958	p_{34}	1.2261	p_{66}	1.2334	p_{98}	-1.8151
p_3	-1.3981	p_{35}	1.4401	p_{67}	1.5338	p_{99}	-1.4829
p_4	0.8481	p_{36}	-0.5988	p_{68}	-0.8844	p_{100}	1.0302
p_5	1.0892	p_{37}	-0.4675	p_{69}	-0.3857	p_{101}	0.9419
p_6	-0.8621	p_{38}	0.8520	p_{70}	0.7730	p_{102}	-1.1472
p_7	1.1512	p_{39}	-0.8922	p_{71}	-0.9754	p_{103}	1.4858
p_8	0.9602	p_{40}	-0.5603	p_{72}	-0.2315	p_{104}	-0.6794
p_9	-1.3581	p_{41}	1.1886	p_{73}	0.5579	p_{105}	0.9573
p_{10}	-0.8354	p_{42}	1.1128	p_{74}	0.4035	p_{106}	1.0807
p_{11}	-1.3249	p_{43}	1.0833	p_{75}	0.4248	p_{107}	1.1445
p_{12}	1.0964	p_{44}	-0.9073	p_{76}	-0.3359	p_{108}	-1.2312
p_{13}	1.3334	p_{45}	-1.6227	p_{77}	-0.9914	p_{109}	-0.6643
p_{14}	-0.7378	p_{46}	1.0013	p_{78}	0.5975	p_{110}	0.3836
p_{15}	1.3565	p_{47}	-1.6067	p_{79}	-0.8408	p_{111}	-1.1482
p_{16}	0.9361	p_{48}	0.3360	p_{80}	0.3587	p_{112}	-0.0353
p_{17}	-0.8212	p_{49}	-1.3136	p_{81}	-0.9604	p_{113}	-0.6747
p_{18}	-0.2662	p_{50}	-1.4447	p_{82}	-1.0002	p_{114}	-1.1653
p_{19}	-0.6866	p_{51}	-1.7238	p_{83}	-1.1636	p_{115}	-0.8896
p_{20}	0.8437	p_{52}	1.0287	p_{84}	0.9590	p_{116}	0.2414
p_{21}	1.1237	p_{53}	0.6100	p_{85}	0.7137	p_{117}	0.1160
p_{22}	-0.3265	p_{54}	-0.9237	p_{86}	-0.6776	p_{118}	-0.6987
p_{23}	1.0511	p_{55}	1.2618	p_{87}	0.9824	p_{119}	0.4781
p_{24}	0.7927	p_{56}	0.5974	p_{88}	-0.5454	p_{120}	0.1821
p_{25}	-0.3363	p_{57}	-1.0976	p_{89}	1.1022	p_{121}	-1.0672
p_{26}	-0.1342	p_{58}	-0.9776	p_{90}	1.6485	p_{122}	-0.9676
p_{27}	-0.1546	p_{59}	-0.9982	p_{91}	1.3307	p_{123}	-1.2321
p_{28}	0.6955	p_{60}	0.8967	p_{92}	-1.2852	p_{124}	0.5003
p_{29}	1.0608	p_{61}	1.7640	p_{93}	-1.2659	p_{125}	0.7419
p_{30}	-0.1600	p_{62}	-1.0211	p_{94}	0.9435	p_{126}	-0.8934
p_{31}	0.9442	p_{63}	1.6913	p_{95}	-1.6809	p_{127}	0.8391

Table 5.2: Time-domain Preamble Pattern 2

Sequence Element	Value	Sequence Element	Value	Sequence Element	Value	Sequence Element	Value
p_0	0.9679	p_{32}	-1.2905	p_{64}	1.5280	p_{96}	0.5193
p_1	-1.0186	p_{33}	1.1040	p_{65}	-0.9193	p_{97}	-0.3439
p_2	0.4883	p_{34}	-1.2408	p_{66}	1.1246	p_{98}	0.1428
p_3	0.5432	p_{35}	-0.8062	p_{67}	1.2622	p_{99}	0.6251
p_4	-1.4702	p_{36}	1.5425	p_{68}	-1.4406	p_{100}	-1.0468
p_5	-1.4507	p_{37}	1.0955	p_{69}	-1.4929	p_{101}	-0.5798
p_6	-1.1752	p_{38}	1.4284	p_{70}	-1.1508	p_{102}	-0.8237
p_7	-0.0730	p_{39}	-0.4593	p_{71}	0.4126	p_{103}	0.2667
p_8	-1.2445	p_{40}	-1.0408	p_{72}	-1.0462	p_{104}	-0.9564
p_9	0.3143	p_{41}	1.0542	p_{73}	0.7232	p_{105}	0.6016
p_{10}	-1.3951	p_{42}	-0.4446	p_{74}	-1.1574	p_{106}	-0.9964
p_{11}	-0.9694	p_{43}	-0.7929	p_{75}	-0.7102	p_{107}	-0.3541
p_{12}	0.4563	p_{44}	1.6733	p_{76}	0.8502	p_{108}	0.3965
p_{13}	0.3073	p_{45}	1.7568	p_{77}	0.6260	p_{109}	0.5201
p_{14}	0.6408	p_{46}	1.3273	p_{78}	0.9530	p_{110}	0.4733
p_{15}	-0.9798	p_{47}	-0.2465	p_{79}	-0.4971	p_{111}	-0.2362
p_{16}	-1.4116	p_{48}	1.6850	p_{80}	-0.8633	p_{112}	-0.6892
p_{17}	0.6038	p_{49}	-0.7091	p_{81}	0.6910	p_{113}	0.4787
p_{18}	-1.3860	p_{50}	1.1396	p_{82}	-0.3639	p_{114}	-0.2605
p_{19}	-1.0888	p_{51}	1.5114	p_{83}	-0.8874	p_{115}	-0.5887
p_{20}	1.1036	p_{52}	-1.4343	p_{84}	1.5311	p_{116}	0.9411
p_{21}	0.7067	p_{53}	-1.5005	p_{85}	1.1546	p_{117}	0.7364
p_{22}	1.1667	p_{54}	-1.2572	p_{86}	1.1935	p_{118}	0.6714
p_{23}	-1.0225	p_{55}	0.8274	p_{87}	-0.2930	p_{119}	-0.1746
p_{24}	-1.2471	p_{56}	-1.5140	p_{88}	1.3285	p_{120}	1.1776
p_{25}	0.7788	p_{57}	1.1421	p_{89}	-0.7231	p_{121}	-0.8803
p_{26}	-1.2716	p_{58}	-1.0135	p_{90}	1.2832	p_{122}	1.2542
p_{27}	-0.8745	p_{59}	-1.0657	p_{91}	0.7878	p_{123}	0.5111
p_{28}	1.2175	p_{60}	1.4073	p_{92}	-0.8095	p_{124}	-0.8209
p_{29}	0.8419	p_{61}	1.8196	p_{93}	-0.7463	p_{125}	-0.8975
p_{30}	1.2881	p_{62}	1.1679	p_{94}	-0.8973	p_{126}	-0.9091
p_{31}	-0.8210	p_{63}	-0.4131	p_{95}	0.5560	p_{127}	0.2562

Table 5.3: Time-domain Preamble Pattern 3

Sequence Element	Value	Sequence Element	Value	Sequence Element	Value	Sequence Element	Value
p_0	0.4047	p_{32}	-0.9671	p_{64}	-0.7298	p_{96}	0.2424
p_1	0.5799	p_{33}	-0.9819	p_{65}	-0.9662	p_{97}	0.5703
p_2	-0.3407	p_{34}	0.7980	p_{66}	0.9694	p_{98}	-0.6381
p_3	0.4343	p_{35}	-0.8158	p_{67}	-0.8053	p_{99}	0.7861
p_4	0.0973	p_{36}	-0.9188	p_{68}	-0.9052	p_{100}	0.9175
p_5	-0.7637	p_{37}	1.5146	p_{69}	1.5933	p_{101}	-0.4595
p_6	-0.6181	p_{38}	0.8138	p_{70}	0.8418	p_{102}	-0.2201
p_7	-0.6539	p_{39}	1.3773	p_{71}	1.5363	p_{103}	-0.7755
p_8	0.3768	p_{40}	0.2108	p_{72}	0.3085	p_{104}	-0.2965
p_9	0.7241	p_{41}	0.9245	p_{73}	1.3016	p_{105}	-1.1220
p_{10}	-1.2095	p_{42}	-1.2138	p_{74}	-1.5546	p_{106}	1.7152
p_{11}	0.6027	p_{43}	1.1252	p_{75}	1.5347	p_{107}	-1.2756
p_{12}	0.4587	p_{44}	0.9663	p_{76}	1.0935	p_{108}	-0.7731
p_{13}	-1.3879	p_{45}	-0.8418	p_{77}	-0.8978	p_{109}	1.0724
p_{14}	-1.0592	p_{46}	-0.6811	p_{78}	-0.9712	p_{110}	1.1733
p_{15}	-1.4052	p_{47}	-1.3003	p_{79}	-1.3763	p_{111}	1.4711
p_{16}	-0.8439	p_{48}	-0.3397	p_{80}	-0.6360	p_{112}	0.4881
p_{17}	-1.5992	p_{49}	-1.1051	p_{81}	-1.2947	p_{113}	0.7528
p_{18}	1.1975	p_{50}	1.2400	p_{82}	1.6436	p_{114}	-0.6417
p_{19}	-1.9525	p_{51}	-1.3975	p_{83}	-1.6564	p_{115}	1.0363
p_{20}	-1.5141	p_{52}	-0.7467	p_{84}	-1.1981	p_{116}	0.8002
p_{21}	0.7219	p_{53}	0.2706	p_{85}	0.8719	p_{117}	-0.0077
p_{22}	0.6982	p_{54}	0.7294	p_{86}	0.9992	p_{118}	-0.2336
p_{23}	1.2924	p_{55}	0.7444	p_{87}	1.4872	p_{119}	-0.4653
p_{24}	-0.9460	p_{56}	-0.3970	p_{88}	-0.4586	p_{120}	0.6862
p_{25}	-1.2407	p_{57}	-1.0718	p_{89}	-0.8404	p_{121}	1.2716
p_{26}	0.4572	p_{58}	0.6646	p_{90}	0.6982	p_{122}	-0.8880
p_{27}	-1.2151	p_{59}	-1.1037	p_{91}	-0.7959	p_{123}	1.4011
p_{28}	-0.9869	p_{60}	-0.5716	p_{92}	-0.5692	p_{124}	0.9531
p_{29}	1.2792	p_{61}	0.9001	p_{93}	1.3528	p_{125}	-1.1210
p_{30}	0.6882	p_{62}	0.7317	p_{94}	0.9536	p_{126}	-0.9489
p_{31}	1.2586	p_{63}	0.9846	p_{95}	1.1784	p_{127}	-1.2566

Table 5.4: Time-domain Preamble Pattern 4

Sequence Element	Value	Sequence Element	Value	Sequence Element	Value	Sequence Element	Value
p_0	1.1549	p_{32}	-1.2385	p_{64}	1.3095	p_{96}	-1.0094
p_1	1.0079	p_{33}	-0.7883	p_{65}	0.6675	p_{97}	-0.7598
p_2	0.7356	p_{34}	-0.7954	p_{66}	1.2587	p_{98}	-1.0786
p_3	-0.7434	p_{35}	1.0874	p_{67}	-0.9993	p_{99}	0.6699
p_4	-1.3930	p_{36}	1.1491	p_{68}	-1.0052	p_{100}	0.9813
p_5	1.2818	p_{37}	-1.4780	p_{69}	0.6601	p_{101}	-0.5563
p_6	-1.1033	p_{38}	0.8870	p_{70}	-1.0228	p_{102}	1.0548
p_7	-0.2523	p_{39}	0.4694	p_{71}	-0.7489	p_{103}	0.8925
p_8	-0.7905	p_{40}	1.5066	p_{72}	0.5086	p_{104}	-1.3656
p_9	-0.4261	p_{41}	1.1266	p_{73}	0.1563	p_{105}	-0.8472
p_{10}	-0.9390	p_{42}	0.9935	p_{74}	0.0673	p_{106}	-1.3110
p_{11}	0.4345	p_{43}	-1.2462	p_{75}	-0.8375	p_{107}	1.1897
p_{12}	0.4433	p_{44}	-1.7869	p_{76}	-1.0746	p_{108}	1.5127
p_{13}	-0.3076	p_{45}	1.7462	p_{77}	0.4454	p_{109}	-0.7474
p_{14}	0.5644	p_{46}	-1.4881	p_{78}	-0.7831	p_{110}	1.4678
p_{15}	0.2571	p_{47}	-0.4090	p_{79}	-0.3623	p_{111}	1.0295
p_{16}	-1.0030	p_{48}	-1.4694	p_{80}	-1.3658	p_{112}	-0.9210
p_{17}	-0.7820	p_{49}	-0.7923	p_{81}	-1.0854	p_{113}	-0.4784
p_{18}	-0.4064	p_{50}	-1.4607	p_{82}	-1.4923	p_{114}	-0.5022
p_{19}	0.9035	p_{51}	0.9113	p_{83}	0.4233	p_{115}	1.2153
p_{20}	1.5406	p_{52}	0.8454	p_{84}	0.6741	p_{116}	1.5783
p_{21}	-1.4613	p_{53}	-0.8866	p_{85}	-1.0157	p_{117}	-0.7718
p_{22}	1.2745	p_{54}	0.8852	p_{86}	0.8304	p_{118}	1.2384
p_{23}	0.3715	p_{55}	0.4918	p_{87}	0.4878	p_{119}	0.6695
p_{24}	1.8134	p_{56}	-0.6096	p_{88}	-1.4992	p_{120}	0.8821
p_{25}	0.9438	p_{57}	-0.4322	p_{89}	-1.1884	p_{121}	0.7808
p_{26}	1.3130	p_{58}	-0.1327	p_{90}	-1.4008	p_{122}	1.0537
p_{27}	-1.3070	p_{59}	0.4953	p_{91}	0.7795	p_{123}	-0.0791
p_{28}	-1.3462	p_{60}	0.9702	p_{92}	1.2926	p_{124}	-0.2845
p_{29}	1.6868	p_{61}	-0.8667	p_{93}	-1.2049	p_{125}	0.5790
p_{30}	-1.2153	p_{62}	0.6803	p_{94}	1.2934	p_{126}	-0.4664
p_{31}	-0.6778	p_{63}	-0.0244	p_{95}	0.8123	p_{127}	-0.1097

Table 5.5: Time-domain Preamble Pattern 5

Sequence Element	Value	Sequence Element	Value	Sequence Element	Value	Sequence Element	Value
p_0	0.9574	p_{32}	0.8400	p_{64}	0.5859	p_{96}	-0.8528
p_1	0.5270	p_{33}	1.3980	p_{65}	0.3053	p_{97}	-0.6973
p_2	1.5929	p_{34}	1.1147	p_{66}	0.8948	p_{98}	-1.2477
p_3	-0.2500	p_{35}	-0.4732	p_{67}	-0.6744	p_{99}	0.6246
p_4	-0.2536	p_{36}	-1.7178	p_{68}	-0.8901	p_{100}	0.7687
p_5	-0.3023	p_{37}	-0.8477	p_{69}	-0.8133	p_{101}	0.7966
p_6	1.2907	p_{38}	1.5083	p_{70}	0.9201	p_{102}	-1.2809
p_7	-0.4258	p_{39}	-1.4364	p_{71}	-1.0841	p_{103}	1.1023
p_8	1.0012	p_{40}	0.3853	p_{72}	-0.8036	p_{104}	0.4250
p_9	1.7704	p_{41}	1.5673	p_{73}	-0.3105	p_{105}	-0.1614
p_{10}	0.8593	p_{42}	0.0295	p_{74}	-1.0514	p_{106}	0.7547
p_{11}	-0.3719	p_{43}	-0.4204	p_{75}	0.7644	p_{107}	-0.6696
p_{12}	-1.3465	p_{44}	-1.4856	p_{76}	0.7301	p_{108}	-0.3920
p_{13}	-0.7419	p_{45}	-0.8404	p_{77}	0.9788	p_{109}	-0.7589
p_{14}	1.5350	p_{46}	1.0111	p_{78}	-1.1305	p_{110}	0.6701
p_{15}	-1.2800	p_{47}	-1.4269	p_{79}	1.3257	p_{111}	-0.9381
p_{16}	0.6955	p_{48}	0.3033	p_{80}	0.7801	p_{112}	-0.7483
p_{17}	1.7204	p_{49}	0.7757	p_{81}	0.7867	p_{113}	-0.9659
p_{18}	0.1643	p_{50}	-0.1370	p_{82}	1.0996	p_{114}	-0.9192
p_{19}	-0.3347	p_{51}	-0.5250	p_{83}	-0.5623	p_{115}	0.3925
p_{20}	-1.7244	p_{52}	-1.1589	p_{84}	-1.2227	p_{116}	1.2864
p_{21}	-0.7447	p_{53}	-0.8324	p_{85}	-0.8223	p_{117}	0.6784
p_{22}	1.1141	p_{54}	0.6336	p_{86}	1.2074	p_{118}	-1.0909
p_{23}	-1.3541	p_{55}	-1.2698	p_{87}	-1.2338	p_{119}	1.1140
p_{24}	-0.7293	p_{56}	-0.7853	p_{88}	0.2957	p_{120}	-0.6134
p_{25}	0.2682	p_{57}	-0.7031	p_{89}	1.0999	p_{121}	-1.5467
p_{26}	-1.2401	p_{58}	-1.1106	p_{90}	-0.0201	p_{122}	-0.3031
p_{27}	1.0527	p_{59}	0.6071	p_{91}	-0.5860	p_{123}	0.9457
p_{28}	0.1199	p_{60}	0.7164	p_{92}	-1.2284	p_{124}	1.9645
p_{29}	1.1496	p_{61}	0.8305	p_{93}	-0.9215	p_{125}	1.4549
p_{30}	-1.0544	p_{62}	-1.2355	p_{94}	0.7941	p_{126}	-1.2760
p_{31}	1.3176	p_{63}	1.1754	p_{95}	-1.4128	p_{127}	2.2102

References

[1] C. R. N. Athaudage, "BER sensitivity of OFDM systems to time synchronization error", in Proc. The 8th International Conference on Communication Systems (ICCS 2002), vol. 1, pp. 42-46, 25-28 Nov. 2002

[2] M. Speth, F. Classen and H. Meyr, "Frame synchronization of OFDM systems in frequency selective fading channels", in Proc. IEEE 47th Vehicular Technology Conference, vol.3, pp. 1807-1811, 4-7 May 1997

[3] P. H. Moose, "A technique for orthogonal frequency division multiplexing frequency offset correction", IEEE Trans. Commnunications, vol. 42, no. 10, pp. 2908-2914, Oct. 1994

[4] T. M. Schmidl and D. C. Cox, "Robust frequency and timing synchronization for OFDM", IEEE Trans. Communications, vol. 45, pp. 1613-1621, Dec. 1997

[5] M. Morelli and U. Mengali, "An improved frequency offset estimator for OFDM applications", IEEE Commns Letter, vol. 3, no. 3, pp. 75-77, Mar. 1999

[6] M. Morelli and U. Mengali, "Frequency ambiguity resolution in OFDM systems", IEEE Commns Letter, vol. 4, no. 4, pp. 134-136, Apr. 2000

[7] M. Morelli and U. Mengali, "Carrier-frequency estimation for transmissions over selective channels", IEEE Trans. Communications, vol. 48, no. 9, pp. 1580-1589, Sep. 2000

[8] H. Minn, V. K. Bhargava and K. B. Letaief, "A Robust Timing and Frequency Synchronization for OFDM Systems", IEEE Trans. Wireless Communications, vol. 2, issue 4, pp. 822-839, Jul. 2003

[9] D. Huang, K. B. Letaief and J. Lu, "Reduced complexity carrier frequency offset estimation for OFDM systems", in Proc. IEEE Wireless Commnunications and Networking Conference (WCNC 2004), vol. 3, pp. 1411-1415, 21-25 Mar. 2004

[10] J. J. Van de Beek, M. Sandell, M. Isaksson, and P. B*ö*rjesson, "Low complex frame synchronization in OFDM systems", in Proc. 4th IEEE International Conference on Universal Personal Communications (ICUPC 1995), pp. 982-986, 6-10 Nov. 1995

[11] Batra, J. Balakrishnan, et al., "Multi-band OFDM physical layer proposal for IEEE P802.15 Task Group 3a", IEEE P802.15-SG3a-03/268r4, IEEE P802.15 Working Group for Wireless Personal Area Networks (WPANs), Mar. 2004

[12] J. R. Foerster, "Channel modeling sub-committee report final", IEEE P802.15-SG3a-02/490r1, IEEE P802.15 Working Group for Wireless Personal Area Networks (WPANS), Feb. 2003

[13] A. Saleh, and R. Valenzuala, "A statistical model for indoor multipath propagation", IEEE Journal on Selected Areas in Communications, vol. SAC-5, no. 2, pp. 128-137, Feb. 1987

[14] J. R. Foerster, A. F. Molisch and M. Pendergrass, "Channel models for Ultrawideband Personal Area Networks", IEEE Wireless Communications [also IEEE Personal Communications], vol. 10, issue. 6, pp. 14-21, Dec. 2003

[15] Chin Wee Yak, Zhongding Lei, Suttinan Chattong and Tjeng Thiang Tjhung, "Timing Synchronization for Ultra-Wideband (UWB) Multi-Band OFDM Systems", in Proc. IEEE 62nd Vehicular Technology Conference (VTC-Fall 2005), vol. 3, pp. 1599-1603, 25-28 Sep. 2005

[16] Chin Wee Yak, Zhongding Lei and Tjeng Thiang Tjhung, "Maximum Likelihood Frequency Offset Estimation & Cramer Rao Bound for Ultra-Wideband (UWB) Multi-Band OFDM Systems", in Proc. IEEE 63rd Vehicular Technology Conference (VTC-Spring 2006), 7-10 May 2006

[17] S. M. Kay, Fundamentals of statistical signal processing, volume I: estimation theory, Prentice Hall, Mar. 1993

[18] D. Rife and R. Boorstyn, "Single-tone parameter estimation from discrete-time observations", IEEE Trans. Inform Theory, vol. IT-20, no. 5, pp. 591-598, Sep. 1974

[19] Chin Wee Yak, Zhongding Lei, Suttinan Chattong and Tjeng Thiang Tjhung, "Timing synchronization and Frequency Offset Estimation for Ultra-Wideband (UWB) Multi-Band OFDM systems", in Proc. IEEE 16th International Symposium on Personal Indoor and Mobile Radio Communications (PIMRC 2005), 11-15 Sep. 2005

[20] Chin Wee Yak, Zhongding Lei and Tjeng Thiang Tjhung, "Ultra-wideband Multi-band OFDM Systems: Timing Synchronization & Frequency Offset Estimation", *submitted and pending acceptance* IEEE Trans. on Wireless Communications

[21] K. Wang, M. Faulkner, J. Singh and I. Tolochko, "A synchronization scheme for OFDM-WLANs", in Proc. 3rd ATcrc Telecommunications and Networking Conference, Dec. 2003

[22] Z. Zhang, M. Zhao, H. Zhou and Y. Liu, "Frequency offset estimation with fast acquisition in OFDM system", IEEE Commns. Letter, vol. 8, no. 3, pp. 171-173, Mar 2004

[23] T. Pollet, M. van Bladel and M. Moeneclaey, "BER sensitivity of OFDM systems to carrier frequency offset and Wiener phase noise", IEEE Trans. Commmunications, vol. 43, no. 2/3/4, pp. 191-193, Feb./Mar./Apr. 1995

[24] A. J. Coulson,"Maximum likelihood synchronization for OFDM using a pilot symbol: analysis", IEEE Jounal Sel. Areas Commns, vol. 19, pp. 2495-2503, Dec. 2001

[25] D. Lee and K. Cheun, "Coarse symbol synchronization algorithms for OFDM systems in multipath channels", IEEE Commns. Letters, vol. 6, no. 10, pp. 446-448, Oct. 2002

[26] K. Shi and E. Serpedin, "A robust metric for coarse frame and carrier synchronization of OFDM systems", in Proc. 36th Asilomar Conference on Signals, Systems and Computers, vol. 2, pp. 1827-1831, 3-6 Nov. 2002

[27] B. Yang, K. B. Letaief, R. S. Cheng and Z. Cao, "Timing recovery for OFDM transmission", IEEE Journal Sel. Areas Commns., vol. 18, no. 11, pp. 2278-2291, Nov. 2000

[28] W. Lei, T. Tao, J. Lu, "A robust frequency acquisition algorithm for OFDM systems", in Proc. 5th International Symposium on Wireless Personal Multimedia Communications, vol. 1, pp. 145-148, 27-30 Oct. 2002

[29] P. Dent, G. E. Bottomley and T. Croft, "Jakes fading model revisited", IEEE Electronics Letters , vol. 29, issue 13, pp. 1162 - 1163, Jun. 1993

[30] W. C. Jakes, Jr., Microwave mobile communications, Wiley-IEEE Press, 2nd Ed., 1994

[31] R. V. Nee and R. Prasad, OFDM for wireless multimedia communications, Artech House, 2000

[32] L. Hanzo, W. Webb and T. Keller, Single- and multi-carrier quadrature amplitude modulation: principles and applications for personal communications, WLANs and Broadcasting, John Wiley & Sons, 2nd Ed., 2000

[33] A. F. Molisch, J. R. Foerster and M. Pendergrass, "Channel models for Ultrawideband personal area networks", IEEE Wireless Communications, vol. 10, issue 6, pp. 14 - 21, Dec. 2003

[34] D. Cassioli, M. Z. Win, A. F. Molisch, "The ultra-wide bandwidth indoor channel: from statistical model to simulations", IEEE Jounal Sel. Areas Commns, vol. 20, issue 6, pp. 1247 - 1257, Aug. 2002

Publications

{1} Chin Wee Yak, Zhongding Lei, Suttinan Chattong and Tjeng Thiang Tjhung, "Timing Synchronization for Ultra-Wideband (UWB) Multi-Band OFDM Systems", in Proc. IEEE 62nd Vehicular Technology Conference (VTC-Fall 2005), vol. 3, pp. 1599-1603, 25-28 Sep. 2005

{2} Chin Wee Yak, Zhongding Lei, Suttinan Chattong and Tjeng Thiang Tjhung, "Timing synchronization and Frequency Offset Estimation for Ultra-Wideband (UWB) Multi-Band OFDM systems", in Proc. IEEE 16th International Symposium on Personal Indoor and Mobile Radio Communications (PIMRC 2005), 11-15 Sep. 2005

{3} Chin Wee Yak, Zhongding Lei and Tjeng Thiang Tjhung, "Maximum Likelihood Frequency Offset Estimation & Cramer Rao Bound for Ultra-Wideband (UWB) Multi-Band OFDM Systems", in Proc. IEEE 63rd Vehicular Technology Conference (VTC-Spring 2006), 7-10 May 2006

{4} Chin Wee Yak, Zhongding Lei and Tjeng Thiang Tjhung, "Ultra-wideband Multi-band OFDM Systems: Timing Synchronization & Frequency Offset Estimation", *submitted and pending* IEEE Trans. on Wireless Communications